

ornl

ORNL/TM-10793

OAK RIDGE
NATIONAL
LABORATORY

MARTIN MARIETTA

Development of Iron Aluminides for Coal Conversion Systems

C. G. McKamey
C. T. Liu
S. A. David
J. A. Horton
D. H. Pierce
J. J. Campbell

*Research supported by the Morgantown Energy
Technology Center, U.S. Department of Energy*

OAK RIDGE NATIONAL LABORATORY

CENTRAL RESEARCH LIBRARY

CIRCULATION SECTION

4075 ROOM 125

LIBRARY LOAN COPY

DO NOT TRANSFER TO ANOTHER PERSON

If you wish someone else to see this
report, send to some with report and
the library will arrange a loan.

10/19/87

OPERATED BY
MARTIN MARIETTA ENERGY SYSTEMS, INC.
FOR THE UNITED STATES
DEPARTMENT OF ENERGY

Fossil
Energy
Program

Printed in the United States of America Available from
National Technical Information Service
U.S. Department of Commerce
5285 Port Royal Road, Springfield, Virginia 22161
NTIS price codes—Printed Copy: A04 Microfiche A01

This report was prepared as an account of work sponsored by an agency of the United States Government. Neither the United States Government nor any agency thereof, nor any of their employees, makes any warranty, express or implied, or assumes any legal liability or responsibility for the accuracy, completeness, or usefulness of any information, apparatus, product, or process disclosed, or represents that its use would not infringe privately owned rights. Reference herein to any specific commercial product, process, or service by trade name, trademark, manufacturer, or otherwise, does not necessarily constitute or imply its endorsement, recommendation, or favoring by the United States Government or any agency thereof. The views and opinions of authors expressed herein do not necessarily state or reflect those of the United States Government or any agency thereof.

DEVELOPMENT OF IRON ALUMINIDES FOR COAL CONVERSION SYSTEMS

C. G. McKamey
C. T. Liu
S. A. David
J. A. Horton
D. H. Pierce
J. J. Campbell

Date Published - July 1988

NOTICE: This document contains information of a preliminary nature. It is subject to revision or correction and therefore does not represent a final report.

Research supported by the
Morgantown Energy Technology Center
Surface Gasification Materials Program
and the
AR&TD Fossil Energy Materials Program

Prepared by
OAK RIDGE NATIONAL LABORATORY
Oak Ridge, Tennessee 37831
operated by
MARTIN MARIETTA ENERGY SYSTEMS, INC.
for the
U.S. DEPARTMENT OF ENERGY
under Contract DE-AC05-84OR21400



3 4456 0289957 6

CONTENTS

LIST OF FIGURES	v
LIST OF TABLES	viii
ABSTRACT	1
1. INTRODUCTION	1
2. BACKGROUND	2
3. EXPERIMENTAL PROCEDURES	8
4. STUDIES ON BINARY ALLOYS	9
4.1 GENERAL CHARACTERIZATION	9
4.2 EFFECT OF STOICHIOMETRY ON MECHANICAL PROPERTIES	13
5. DEVELOPMENT OF ALUMINIDE ALLOYS	19
5.1 FABRICABILITY	21
5.2 MICROSTRUCTURES	21
5.2.1 Ternary Alloys	21
5.2.2 Multicomponent Alloys	26
5.3 TENSILE PROPERTIES	32
5.3.1 Ternary Alloys	32
5.3.2 Multicomponent Alloys	34
5.4 FRACTURE SURFACES	37
5.5 CREEP PROPERTIES	37
5.6 OXIDATION RESISTANCE	40
5.7 WELDABILITY	41
6. SUMMARY	42
7. REFERENCES	47

LIST OF FIGURES

Fig. 1. The iron-aluminum phase diagram showing the phases of interest to this study 4

Fig. 2. Schematic illustration of possible DO_3 superlattice dislocations and their imperfect variants 5

Fig. 3. Tensile properties of iron aluminides as functions of aluminum concentration. (a) Yield strength. (b) Ductility 10

Fig. 4. Appearance of iron aluminides of 24-27% Al after exposure to sulfidizing atmosphere for 168 h at 700 and 871°C 12

Fig. 5. Room-temperature yield strength and elongation vs composition of iron aluminides 14

Fig. 6. A $\langle 111 \rangle$ dark-field transmission electron micrograph of Fe-24% Al showing its two-phase nature: bright regions are ordered DO_3 phase; dark regions are disordered α phase 14

Fig. 7. Transmission electron micrographs of Fe-26% Al. (a) $\langle 111 \rangle$ dark field showing both DO_3 and B2 APBs. (b) $\langle 222 \rangle$ dark field showing only B2 APBs. (c) $\langle 200 \rangle$ dark field showing $\langle 111 \rangle$ faults between dislocations. (d) Bright field showing curved APB ending in a dislocation 17

Fig. 8. Yield stress of iron aluminides vs test temperature and comparison to modified 9Cr-1Mo and type 316 SS 18

Fig. 9. Ductility vs temperature for Fe-28% Al compared with modified 9Cr-1Mo and type 316 SS 19

Fig. 10. As-rolled microstructures of several iron-aluminum alloys. (a) FA-37 base alloy, (b) FA-72, (c) FA-91, and (d) FA-84. All micrographs are 100X 22

Fig. 11. Microstructures of binary and ternary alloys with and without TiB_2 after recrystallization at 850°C and an ordering heat treatment at 500°C. (a) Base alloy FA-37, Fe-28% Al with TiB_2 . (b) FA-64, with 4% Cr and TiB_2 . (c) FA-69, with 4% Mn and TiB_2 . (d) FA-61, base alloy without TiB_2 . (e) FA-72, with 4% Cr and no TiB_2 . (f) FA-71, with 4% Mn and no TiB_2 . All micrographs are 100X . . 23

Fig. 12. Microstructures of several ternary alloys (all with TiB_2) after recrystallization at 850°C and an ordering heat treatment at 500°C. (a) FA-56, with 2% Mo. (b) FA-59, with 1% Nb. (c) FA-54, with 2% Zr. (d) FA-58, with 0.03% Ce. All micrographs are 100X 24

Fig. 13. Microstructures of several multicomponent alloys with chromium as the major alloying addition, after recrystallization at 850°C and an ordering heat treatment at 500°C. (a) FA-84. (b) FA-89. (c) FA-90. (d) FA-98. All micrographs are 100X	27
Fig. 14. Microstructures of multicomponent alloys with molybdenum as the major alloying addition, after recrystallization at 850°C and an ordering heat treatment at 500°C. (a) FA-73. (b) FA-91. (c) FA-92. All micrographs are 100X	28
Fig. 15. Microstructures of multicomponent alloys with chromium and niobium as the major alloying additions, after recrystallization at 850°C and an ordering heat treatment at 500°C. (a) FA-81. (b) FA-93. All micrographs are 100X	29
Fig. 16. Microstructures of multicomponent alloys with chromium and molybdenum as the major alloying additions, after recrystallization at 850°C and an ordering heat treatment at 500°C. (a) FA-85. (b) FA-95. (c) FA-86. All micrographs are 100X	30
Fig. 17. Microstructures of multicomponent alloys with chromium, molybdenum, and niobium as the major alloying additions, after recrystallization at 850°C and an ordering heat treatment at 500°C. (a) FA-96. (b) FA-97. All micrographs are 100X	31
Fig. 18. Room-temperature yield strength of the base alloy FA-37 and ternary iron aluminides, with and without TiB ₂	33
Fig. 19. Room-temperature ductility of the base alloy FA-37 and ternary iron aluminides, with and without TiB ₂	33
Fig. 20. Yield strength at 600°C of the base alloy FA-37 and ternary iron aluminides, with and without TiB ₂	35
Fig. 21. Room-temperature yield strength of the base alloy FA-37 and multicomponent alloys	35
Fig. 22. Room-temperature ductility of the base alloy FA-37 and multicomponent alloys	36
Fig. 23. Yield strength at 600°C of the base alloy FA-37 and multicomponent alloys	36
Fig. 24. Fracture surfaces of several alloys tested in tension. (a) FA-37, 500X. (b) FA-56, 500X. (c). FA-61, 100X. (d) FA-62, 100X	38
Fig. 25. Fracture surface in tension of FA-60 containing TiB ₂ and extra boron showing the effect of boron on the fracture mode of the base alloy. Compare with Fig. 24(a). 500X	39

Fig. 26. Fracture surface in tension of FA-94 (containing no TiB ₂) showing numerous precipitates. 1000X	39
Fig. 27. Oxidation resistance of several iron-aluminum-based alloys at 800°C and comparison with type 316 SS	41
Fig. 28. The effect of the addition of TiB ₂ on the electron-beam weldability of Fe-28% Al. (a) Hot cracking along the fusion line with addition of TiB ₂ . (b) No cracking when TiB ₂ is absent . . .	43
Fig. 29. (a) Typical surface and (b) transverse microstructures of the electron-beam weld in FA-83 made at 25.4 cm/min . .	44

LIST OF TABLES

Table 1.	Oxidation of iron aluminides	11
Table 2.	Alloying agents currently being studies	20
Table 3.	Alloys currently being studied	20
Table 4.	Effect of alloying additions on grain size of Fe ₃ Al with and without TiB ₂	25
Table 5.	Creep properties of iron aluminide alloys	40
Table 6.	Weldability of iron aluminides	42

DEVELOPMENT OF IRON ALUMINIDES FOR COAL CONVERSION SYSTEMS*

C. G. McKamey, C. T. Liu, S. A. David, J. A. Horton,
D. H. Pierce, and J. J. Campbell

ABSTRACT

A study is under way to develop iron aluminide alloys based on Fe_3Al with an optimum combination of strength, ductility, and corrosion resistance for use as hot components in advanced fossil energy conversion systems. The study to date has included two phases: (1) properties of Fe-Al-based compositions between 24 and 30% Al were studied and an evaluation made of their potential for further alloy development; and (2) one binary alloy was chosen for further alloy development and property characterization. Studies include fabricability, microstructure, tensile properties, oxidation and sulfidation resistance, and weldability.

This report summarizes the results of the two phases of work described above. A discussion of the effect of aluminum concentration on mechanical properties of the binary alloys prepared in phase 1 of this study is included. From the results of phase 1, it was determined that Fe-28 at. % Al is the most promising alloy for further development. Initially, 0.5 wt % TiB_2 (~1 at. %) was added for grain refinement. It has since been determined that not only are the TiB_2 precipitates deleterious to the weldability, but that grain refinement can be produced by the addition of other elements. Therefore, the addition of TiB_2 was halted after the initial studies of the effects of ternary additions. In phase 2, additions of chromium, niobium, boron, and molybdenum were shown to improve high-temperature strength, room-temperature ductility, and creep resistance. The results of weldability, tensile, and creep tests, as well as the present status of oxidation and corrosion studies, are reported.

1. INTRODUCTION

The objective of this task is to develop low-cost, low-density intermetallic alloys based on Fe_3Al with an optimum combination of

*Research supported by the U.S. Department of Energy, Morgantown Energy Technology Center, Surface Gasification Materials Program, and the AR&TD Fossil Energy Materials Program, under contract DE-AC05-84OR21400 with Martin Marietta Energy Systems, Inc.

strength, ductility, and corrosion resistance for use as components in advanced fossil energy conversion systems. Initial emphasis has been on the development of iron aluminides for heat recovery applications in coal gasification systems. Iron aluminides near the Fe_3Al composition are expected to be resistant to corrosion in high-temperature fossil energy systems because of their ability to form protective aluminum oxide scales. Currently, however, their usefulness is limited by their low room-temperature ductility (<5%) and poor hot strength above 600°C. The current efforts of this task focus on developing alloys with base compositions near Fe_3Al that have improved hot strength and room-temperature ductility, while retaining the oxidation and corrosion properties of the base alloy.

In previous reports,¹⁻³ we have presented results of our preliminary study of the fabricability, microstructures, mechanical properties, oxidation and sulfidation properties, and weldability of several binary alloys near the Fe_3Al composition. Since the completion of that work, our program has centered on two technical tasks: (1) a more in-depth study of the correlation between aluminum content, microstructure, and mechanical properties in binary iron-aluminum alloys of 24-30 at. % Al; and (2) the effect of macroalloying (<10 at. %) and microalloying (<1 at. %) on the metallurgical and mechanical properties of our selected base alloy, Fe-28 at. % Al.* This report briefly summarizes the results of our early work on binary iron aluminides and describes recent results of the two tasks noted above.

2. BACKGROUND

Currently, most heat-resistant alloys are either nickel-based or high-nickel-content steels containing a delicate balance of one or more strategic elements such as chromium, cobalt, and tungsten to produce the desired properties. In spite of their high degree of development, these state-of-the-art alloys do not have the desired characteristics for the hot components of advanced fossil energy conversion systems, because of their susceptibility to aging embrittlement, to chromium evaporation at

*Throughout this report all compositions are reported in atomic percent unless otherwise noted.

high temperatures, and to catastrophic hot corrosion in sulfur-containing environments. Because of their resistance to the formation of low-melting eutectics and their ability to form a protective aluminum oxide film at very low oxygen partial pressures, iron aluminides near the Fe_3Al composition exhibit excellent corrosion resistance at high temperatures in such environments. Their high strength at room temperature, lower density, and lower cost are also advantages to their use. However, their usefulness for structural applications is currently limited by their low room-temperature ductility (1-5%) and their poor hot strength above 600°C .

Studies of the phase relationships in the Fe-Al system near Fe_3Al have resulted in the phase diagram shown in Fig. 1. The following phase regions have been confirmed:⁴⁻⁶ a disordered solid solution (α), ordered FeAl (B2), ordered Fe_3Al (DO_3), and the two phase regions, $\alpha+\text{DO}_3$ and $\alpha+\text{B2}$, with the boundaries shown in Fig. 1. Two versions of the phase diagram are proposed that are in agreement with respect to the shape of the various phase fields, but in disagreement on the location of the boundaries. Allen and Cahn^{7,8} concluded from thermodynamic considerations and critical experiments that both versions presented in Fig. 1 were correct; the diagram according to Oki, Hasaka, and Eguchi being the metastable one, while the Okamoto and Beck⁶ version was the true equilibrium diagram. This apparent discrepancy, according to Allen and Cahn,^{7,8} arose from the initial generation of large coherency strains between α and the ordered phases that constricted the two phase fields and depressed the miscibility gap. Upon relaxation of the stresses by long equilibration anneals, the two phase regions expand to the boundaries found by Okamoto and Beck.⁶

The tensile behavior of Fe_3Al -based alloys has a strong dependence on temperature, composition, and heat treatment.⁹⁻¹² The yield stress (σ_y) near the Fe_3Al composition increases with temperature above 300°C to a maximum value near 550°C and then decreases sharply. This temperature corresponds to the second-order phase transformation temperature between the DO_3 and the B2 ordered structures.^{4,6} Morgand et al.¹³ showed that this peak in yield stress occurs clearly at compositions from about 23 to 32% Al, which coincides with the composition range of the DO_3 phase. This type of yield behavior has been observed in many other ordered systems,

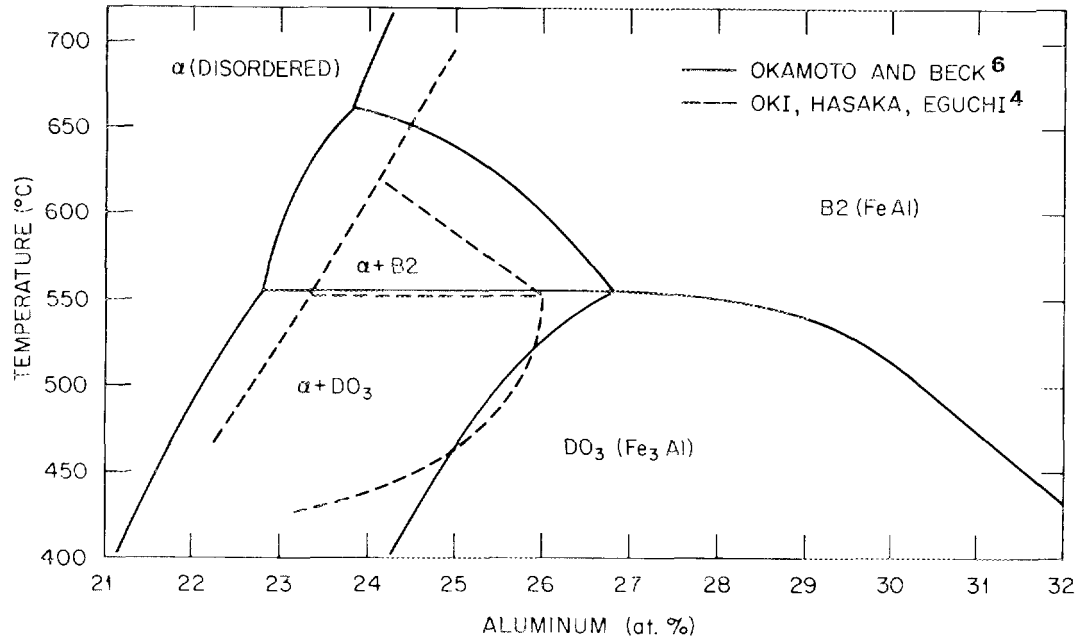


Fig. 1. The iron-aluminum phase diagram showing the phases of interest to this study.

including Ni_3Al (ref. 14), $FeCo$ (ref. 10), $CuZn$ (ref. 15), and Ni_3Mn (ref. 16). Conflicting explanations for its occurrence in Fe_3Al are given in numerous reports. Different mechanisms have been proposed to explain the presence of the yield stress peak as a function of temperature, including the cross-slip model proposed by Kear and Wilsdorf¹⁷ and Takeuchi and Kuramoto¹⁸ and a change in dislocation configuration with degree of order proposed by Stoloff and Davies.¹⁹ However, none of the proposed mechanisms appears to be entirely applicable to the Fe_3Al system.

Within the DO_3 structure, the possible superlattice dislocations and their imperfect variants are shown in Fig. 2 (refs. 9, 20, and 21). Associated with the imperfect variants will be deformation-induced antiphase boundary (APB) trails [Fig. 2(d-f)]. Because the motion of the imperfect types leads to the formation of nearest-neighbor and next-nearest-neighbor APBs (NNAPBs and NNNAPBs), these configurations are mobile only when the magnitude of the external stress is sufficient to

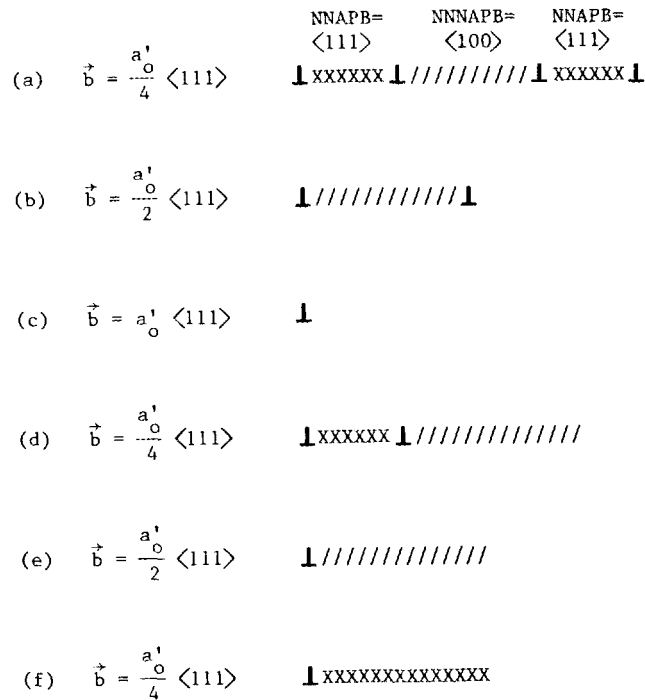


Fig. 2. Schematic illustration of possible DO₃ superlattice dislocations and their imperfect variants.

allow for production of APBs. At compositions of 24–26% Al, single dislocations, sometimes with trailing APBs [similar to Fig. 2(e) and (f)], have been shown to be responsible for the deformation.¹¹ At higher aluminum levels, deformation is thought to occur by APB-coupled dislocations.¹¹ The change in dislocation character results from a change in APB energy. As the aluminum content increases, the energy of the DO₃ APB (NNNAPB) decreases and the B2 APB (NNAPB) energy increases,^{20,21} resulting in twofold superdislocations as shown in Fig. 2(b). There is one report of the existence of fourfold superlattice dislocations [Fig. 2(a)] at compositions from 25–30% Al (ref. 22).

Although iron-aluminum alloys have been studied since the early 1900s, relatively little information on the effect of ternary additions on the mechanical and physical properties of Fe₃Al is available. Because of the brittleness of alloys with higher aluminum levels,^{23,24} early studies concentrated on alloys with less than 20% Al. Recently, more interest has

centered on the Fe_3Al - and FeAl -based ternary alloys because of the improved corrosion resistance at high temperatures that the higher aluminum levels provide. Justusson et al.²⁵ reported a slight strengthening, accompanied by a loss of room-temperature ductility, for small additions of titanium to Fe_3Al . Athanassiadis et al.²⁶ and Mendiratta and Lipsitt²⁷ used transmission electron microscopy (TEM) to study the effect of ternary additions on the D0_3 to B2 transformation temperature. Horton et al.²⁸ found that additions of boron had no effect on the ductility and fracture mode of Fe_3Al and that additions of silicon and copper severely embrittled the alloy by a process of second-phase precipitation. They also reported that nickel additions resulted in alloys that failed intergranularly, except for an alloy of composition Fe-40Ni-20Al .

Several reports were written in the 1950s and 1960s describing the properties of an alloy called Thermenol developed by the Naval Ordnance Laboratory. This alloy contained 28% Al and ~2% Mo plus small amounts (<1%) of zirconium and carbon. Thermenol was reported to have excellent oxidation and corrosion resistance, good stress-rupture and tensile strength at elevated temperatures, soft magnetic characteristics similar to some nickel-based alloys, and high electrical resistivity.²⁹⁻³² However, no significant commercialization occurred, because of low room-temperature ductility and difficulties with processing and control of microstructure.

A recent program sponsored by the Materials Laboratory, Wright-Patterson Air Force Base, in which the contractor was United Technologies Corporation, Pratt and Whitney Aircraft, Government Products Division, addressed the development of iron-aluminide base alloys using rapid solidification.³³ Powders were produced by the Pratt and Whitney-developed RSR (rapid-solidification-rate) process and then consolidated by hot extrusion. Following consolidation, specimens for study were produced by hot and warm working. One of the most important developments to come from this program was the result that Fe_3Al alloys containing TiB_2 precipitates could achieve room temperature tensile-elongation values in the range 15 to 20% with tensile strengths of 965 MPa (140 ksi). The creep rupture strength at 982°C was about equal to that of Hastelloy X. Variations in

consolidation and working conditions and the use of fine vs coarse powder caused variations in the microstructure, which were found to be the major reason for variations in strength and ductility. In general, the finer grain structures produced the best combination of mechanical properties.

Culbertson and Kortovich³⁴ reported the results of their alloy development program involving the addition of certain amounts of titanium, vanadium, chromium, manganese, nickel, niobium, molybdenum, tantalum, copper, or silicon on mechanical properties, workability, and oxidation resistance of Fe₃Al. Their alloys were prepared by Pratt and Whitney, using the RSR process described above, as well as isothermal forging processing procedures. Oxidation tests involved exposures in laboratory air at 816°C. Visual- and weight-change results indicated that only two alloys (5% Ti and 10% V) exhibited significant loss of oxidation resistance, compared with the Fe₃Al base material. Workability testing, involving upset isothermal forging at 954°C, indicated no adverse effects in any of the alloys tested. Improvements in room-temperature yield strength, as measured by tensile testing, were obtained with additions of up to 5% niobium or tantalum. At 600°C, significant increases in yield strength were produced by additions of silicon, tantalum, molybdenum, niobium, or chromium. However, all additions except chromium produced a significant drop in room-temperature ductility, compared with the 5% ductility of Fe₃Al. A strong solid-solution strengthening effect at high temperatures in an alloy with small additions of molybdenum and chromium was noted.

Diehm and Mikkola³⁵ have investigated the effect of the addition of 1.9% Mo and 3.9% Ti on the yield strength and work-hardening rate of Fe₃Al as well as the temperature of the D0₃ to B2 transformation. They note that the deformation behavior is determined largely by the stability of the D0₃ structure relative to the B2 structure and that, by adding elements that increase the transformation temperature, the anomalous peak in yield strength can be pushed to higher temperatures. Examination by TEM indicated that room-temperature deformation is by $\frac{1}{2}\langle 111 \rangle$ dislocation pairs, which create NNNAPBs. At 650°C, deformation is by motion of $\frac{1}{4}\langle 111 \rangle$ unit dislocations and at 800°C, by the $\frac{1}{2}\langle 100 \rangle$ type characteristic of the B2

structure. However, the addition of more solute or a change in the aluminum concentration can cause the appearance of $\langle 110 \rangle$ -type dislocations in the $D0_3$ structure.

An excellent detailed review of the research and development of iron-aluminum based alloys was recently compiled by R. E. Hook (ARMCO, Middleton, Ohio, unpublished data).

3. EXPERIMENTAL PROCEDURES

All alloys used in this study were prepared by arc-melting under argon and drop-casting into water-cooled copper molds. After homogenizing for 5 h at 1000°C , the alloys were hot-rolled to a thickness of ~ 0.9 mm, starting at 1000°C and finishing at 650°C . Final warm rolling to ~ 0.76 mm was done at 600°C .

Tensile samples with a gage section of $0.76 \times 3.18 \times 12.70$ mm were punched from the rolled sheet. After a standard heat treatment of 1 h at 850°C (for recrystallization) plus 7 d at 500°C (for $D0_3$ ordering), tensile tests were conducted in air on an Instron testing machine at a strain rate of $3.3 \times 10^{-3} \text{ s}^{-1}$. The creep properties of selected iron-aluminide alloys were determined at a stress of 207 MPa (30 ksi) at 593°C in air. The temperature was monitored by a platinum vs Pt-10% Rh thermocouple located at the center of the gage section, and the creep elongation was measured using a dial gage.

Oxidation studies were performed on rectangular samples measuring ~ 10 by ~ 15 mm, cut from the 0.76-mm-thick rolled sheet. The samples were prepared for testing by mechanically polishing with 4-0 emery paper, followed by annealing in vacuum for 1 h at 800°C . Air-oxidation tests were then performed at 800 and 1000°C for a total exposure time of 500 h. Measurements of the weight gain as a function of time indicated the degree of oxidation.

Samples of selected alloys were cut from the rolled sheet in 10- by 10-mm squares for sulfidation studies. Surfaces were cleaned as noted above and annealed for 1 h at 800°C in dry hydrogen. The cleaned samples were wrapped in platinum foil, sealed in evacuated capsules containing CaSO_4 , and soaked at 700°C for 168 h. Additional tests were done at 871°C to produce a higher sulfur gas pressure.

Samples for preliminary welding studies were prepared by mechanically polishing as above, then heat treating in vacuum for 1 h at 850°C plus 7 d at 500°C. Both autogeneous electron beam (EB) and gas tungsten arc (GTA) welding procedures were used.

Specimens were prepared for TEM by spark-discharge machining 3-mm disks from the 0.76-mm tensile samples, grinding to a thickness of 0.3 mm, and electropolishing in one part nitric acid to four parts methanol in a Struers Tenupol jet polishing unit at -28°C. Electron microscopy was performed in a Philips EM430.

Optical metallography was performed on specimens etched in a solution of 40 ml HNO₃, 60 ml CH₃COOH, and 20 ml HCl. Grain sizes were determined by the method of linear intercepts.

4. STUDIES ON BINARY ALLOYS

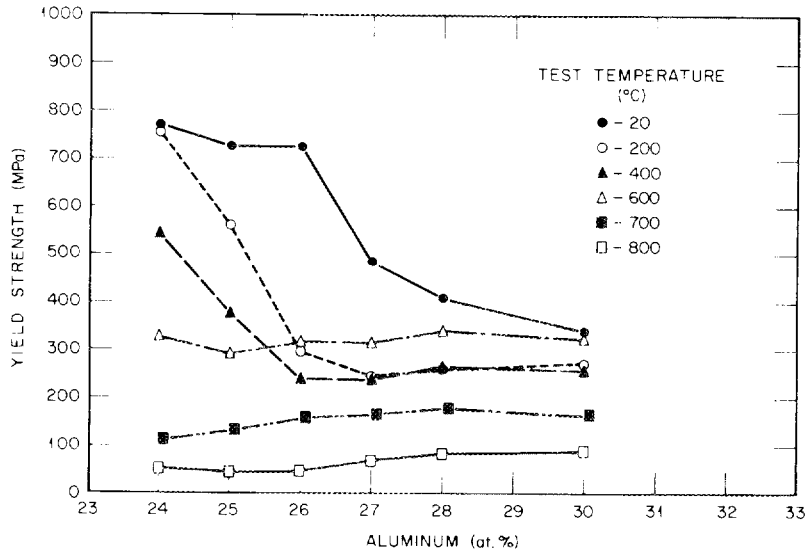
4.1 GENERAL CHARACTERIZATION

In previous reports,¹⁻³ we have presented results of our studies of the fabricability, microstructures, mechanical properties, oxidation and sulfidation resistance, and weldability of several binary alloys near the Fe₃Al composition. This section summarizes only the results of those studies on alloys of 24-30% Al to which 0.5 wt % TiB₂ (≈1 at. %) had been added for grain refinement.

Figure 3 shows the tensile properties of iron aluminide as functions of aluminum concentration and test temperature. At room temperature, the 0.2% yield stress was highest for the 24 to 26% Al alloys (≈750 MPa) and then decreased rapidly to about 350 MPa for the 30% Al alloy. The same trend was observed for samples tested at 200 and 400°C, although stress levels were lower. The decrease in yield stress with aluminum content from 24 to 27% is discussed in the next section, in terms of a change in dislocation structure from unit dislocations to superlattice dislocations. At test temperatures of 600 to 800°C, the opposite trend was observed: the lower aluminum-content alloys exhibited a slightly lower yield strength.

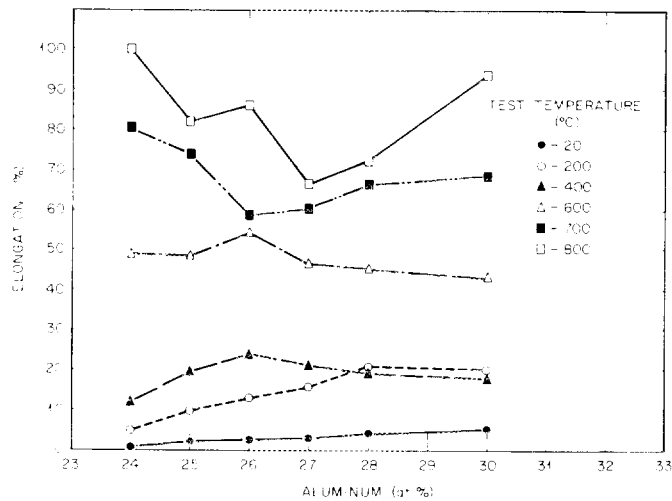
The ductility shown in Fig. 3(b) is also dependent on aluminum content and test temperature. The 24% alloy exhibited a tensile elongation of about ~1% at room temperature. With increasing aluminum

ORNL-DWG 86-15132



(a)

ORNL-DWG 86-15137



(b)

Fig. 3. Tensile properties of iron aluminides as functions of aluminum concentration. (a) Yield strength. (b) Ductility.

concentration, the elongation reached ~5% for the 30% alloy. A sharp increase in ductility was observed with test temperature above 400°C, reaching 50% at 600°C. Because of the excellent hot ductilities, there is no difficulty in fabricating these alloys above 600°C.

Preliminary oxidation studies were conducted on several binary iron aluminides near the Fe₃Al composition. The tests were performed at 800 and 1000°C for ~500 h. Table 1 presents the results of these tests and compares the oxidation resistance of the iron aluminides with that of type 316 SS under the same test conditions. After 526 h at 800°C, all iron aluminides had a dull bluish gray color, with no apparent spalling, and weight gains <0.5 mg/cm². Type 316 SS, on the other hand, had gained ~1.2 mg/cm² at 120 h, when it began to spall. After ~520 h, it showed a net weight gain of 0.95 mg/cm². At 1000°C, weight gains for the aluminides were still low (<0.6 mg/cm²), while the type 316 SS had begun to spall badly. The ability of the iron aluminides to form a protective oxide film is quite evident in these studies.

Table 1. Oxidation of iron aluminides

Alloy	Composition (at. % Al)	Weight change after 526-h exposure (mg/cm ²)	
		800°C	1000°C
FA-36	24	0.45	0.45
FA-40	25	0.46	0.54
FA-38	26	0.45	0.45
FA-41	27	0.43	0.54
FA-39	30	0.14	0.47
Type 316 SS		0.95	-151.68

Sulfidation tests were conducted on alloys of 24 to 27% Al at 700 and 871°C for 168 h. Attack at 700°C was minimal (<0.05 mg/cm²), the oxide scale on all alloys being in the interference color range (Fig. 4). At 871°C, all alloys were covered with a uniform gray coating of oxide and weight gains were 0.22 to 0.27 mg/cm². These results clearly indicate that iron aluminides near Fe₃Al are very resistant to sulfur-containing environments.

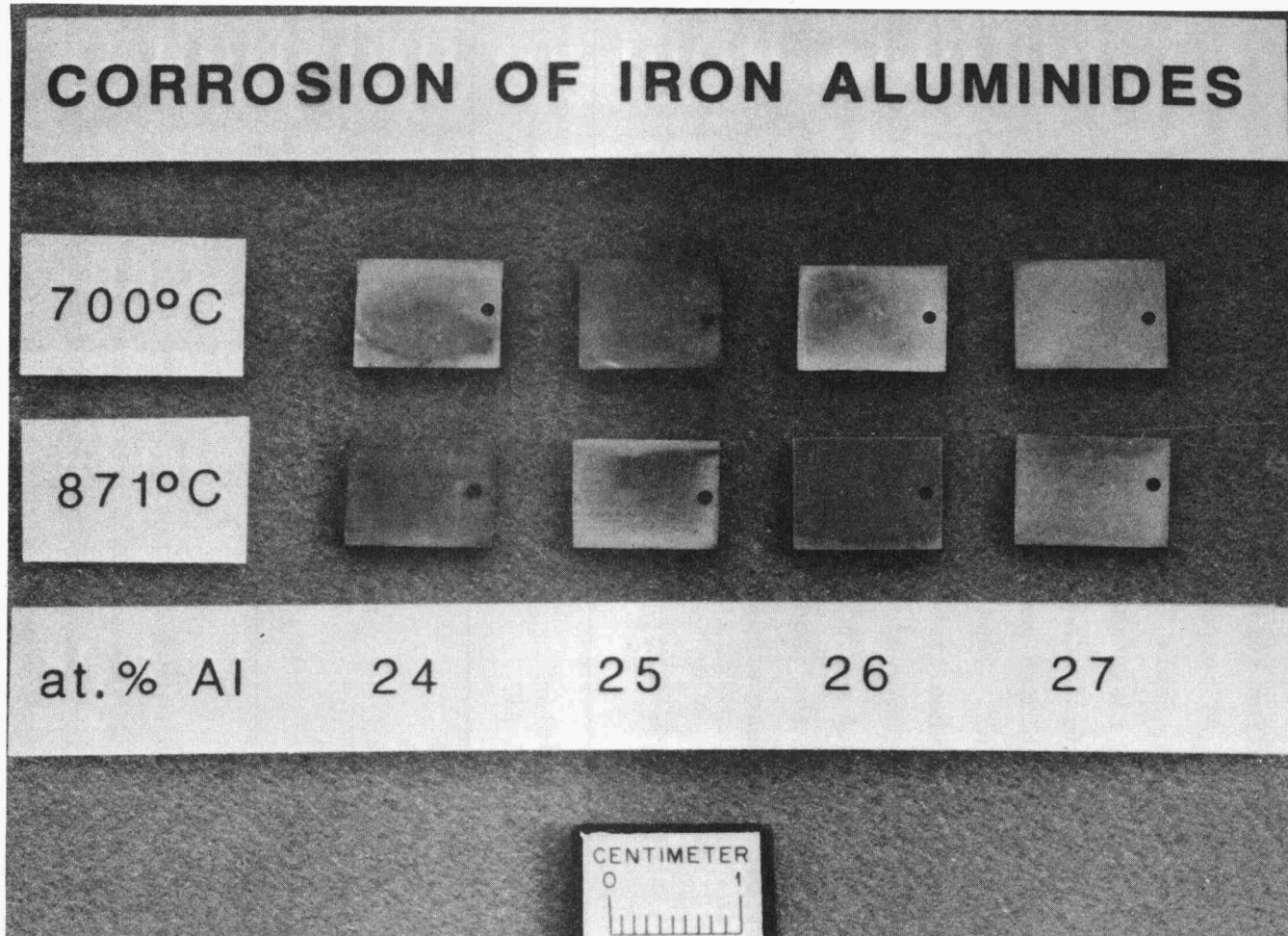


Fig. 4. Appearance of iron aluminides of 24-27% Al after exposure to sulfidizing atmosphere for 168 h at 700 and 871°C.

Preliminary weldability results indicated that the alloys with the highest aluminum content had the best weldability. Transverse or crater cracks occasionally formed in the fusion and heat-affected zones, especially in alloys with lower aluminum content.

The results of phase 1 indicated that alloys of 24 to 30% Al with small additions of TiB_2 could be fabricated by routine, low-cost melting, casting, and rolling procedures. A self-protecting oxide layer, which forms during annealing under low oxygen pressures, provided excellent oxidation and sulfidation resistance. The tensile strengths were higher than those for type 316 SS at temperatures below $760^\circ C$ and for modified 9Cr-1Mo steel at temperatures above $550^\circ C$. The room-temperature ductility increased with the addition of aluminum. Our preliminary weldability studies indicated that the alloys with higher aluminum content had fewer cracks in the fusion and heat-affected zones. On the bases of fabricability, strength, ductility, corrosion resistance, and weldability considerations, the Fe-28% Al alloy was chosen as the base alloy for further development.

4.2 EFFECT OF STOICHIOMETRY ON MECHANICAL PROPERTIES

Figure 5 shows the room-temperature tensile properties as a function of stoichiometry near Fe_3Al . The 0.2% yield strength (σ_y) was highest for the 24-26% Al alloys (≈ 750 MPa) and then decreased rapidly to ~ 350 MPa for the 30% Al alloy. This transition from high σ_y values to lower values around 26% Al coincides with the boundary between the $\alpha+D0_3$ and $D0_3$ phase fields (see Fig. 1) at $\approx 500^\circ C$ (the temperature used for our ordering heat treatment). Previous studies have shown that, at this temperature, compositions near 24% can be age-hardened by precipitation of disordered α from the ordered $D0_3$ phase.³⁶ Our heat treatment at $500^\circ C$ for 7 d was sufficient to cause this reaction to occur, as indicated by the presence of the disordered α phase between ordered thermal $D0_3$ domains in the TEM micrograph shown in Fig. 6. Dark-field images using $\langle 111 \rangle$ and $\langle 002 \rangle$ diffraction vectors show the dark regions to be disordered and the bright regions ordered. Alloys of 26% Al and higher do not age-harden at $500^\circ C$, because they lie outside the $\alpha+D0_3$ phase field at that temperature.³⁶

ORNL-DWG 86-17615

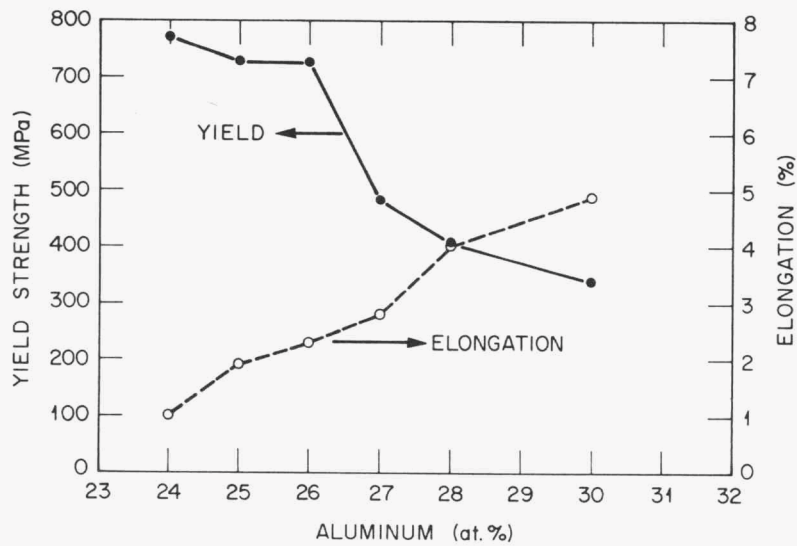


Fig. 5. Room-temperature yield strength and elongation vs composition of iron aluminides.

YE-13398

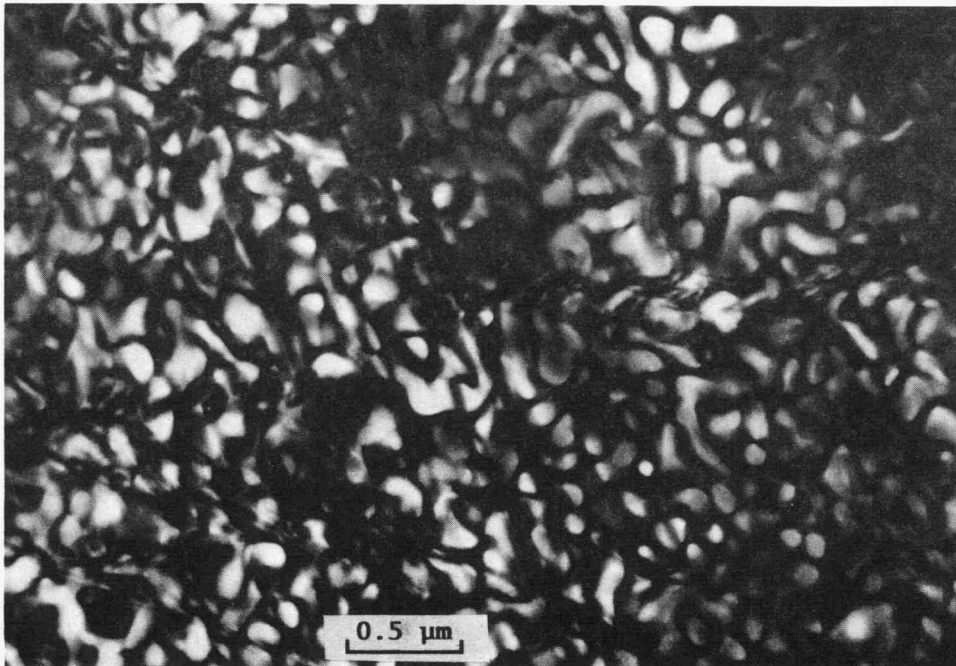


Fig. 6. A $\langle 111 \rangle$ dark-field transmission electron micrograph of Fe-24% Al showing its two-phase nature: bright regions are ordered DO_3 phase; dark regions are disordered α phase.

The higher room temperature strength of alloys near 24% Al may therefore be related to the presence of both disordered and ordered phases (i.e., a precipitation hardening effect).

Figure 5 also shows that the ductility exhibited a fourfold increase from 1% at 24% Al to 5% at 30% Al. This increased ductility corresponds to the decreased yield stress with increasing aluminum content. Note that all the alloys in this study exhibited essentially intergranular fracture,³ and this behavior was not affected by the increase in aluminum content.

In terms of dislocation structures, the studies of Stoloff and Davies,¹⁰ Morgand et al.,¹³ Saburi et al.,¹¹ and Mendiratta et al.³⁷ show that the 24–26% Al composition is in the range where the dislocation mode changes from the glide of single $\frac{1}{4}a_0'$ <111> dislocations (where a_0' is the lattice parameter for the DO_3 structure) associated with the α phase to glide of $\frac{1}{4}a_0'$ <111> dislocation pairs in the DO_3 superlattice. However, any possible fault contrast associated with slip dislocations in the 24 and 25% Al samples of this study were obscured by the small scale of the ordered and disordered regions. The sharp decrease in σ_y with increasing aluminum above 26% is due to the formation of paired dislocations {i.e., superlattice dislocations [as in Fig. 2(d)]} which glide easily in the ordered DO_3 lattice.³⁸

Dislocation and APB types were studied by TEM as a function of composition. The different types of dislocations and APBs can be distinguished in TEM by using the appropriate diffraction conditions.³⁹ Imaging with a <111> superlattice diffraction vector will give rise to contrast from both the NNAPB and NNNAPB trails, while a superlattice diffraction vector of <002> or <222> will give rise to contrast only from NNAPB trails. Also, it has been shown by Crawford and Ray²² that, as the aluminum content increases, the APB energy associated with the DO_3 order (NNNAPB) decreases, while the APB energy associated with the B2 order (NNAPB) increases. Therefore, the number of superlattice dislocations which trail <111> APB faults are expected to decrease with an increase in aluminum level, while those which trail <100> faults should increase.

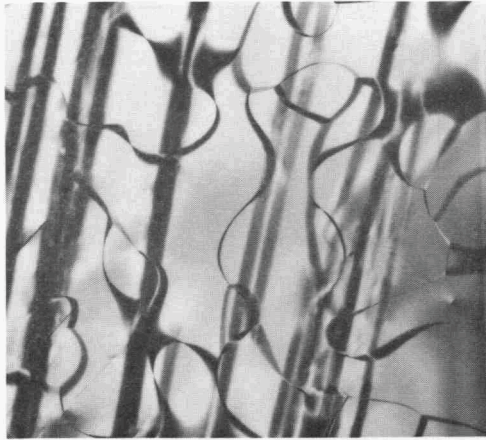
As noted above, the 24% Al alloy exhibited a two-phase structure and the dislocations were obscured by the scale of the APBs (Fig. 6). At 26% Al, which was single phase (DO_3), thermal APBs of both B2 and DO_3 ordering were observed [Fig. 7(a and b)]. Most of the slip dislocations were coupled with a $\langle 111 \rangle$ fault with dislocation separation generally greater than $0.5 \mu\text{m}$ [Fig. 7(c)]. Some of the curved $\langle 100 \rangle$ faults, which were originally thought to be thermally produced, were seen to terminate in dislocations [Fig. 7(d)], suggesting they were deformation induced. The presence of both kinds of deformation-induced faults was expected, because it has been shown that the energies of the two types of APB are about equal at this composition.²²

Thermal APBs with a fault vector of $\langle 100 \rangle$, which results from the DO_3 order, were present in the 28–30% aluminum alloys, but no $\langle 111 \rangle$ thermal faults were seen. Any coupling of dislocations by a $\langle 111 \rangle$ fault was generally not resolvable, in agreement with the expected higher APB energy of the $\langle 111 \rangle$ fault. Movement is, therefore, by one $\frac{1}{2}a_0' \langle 111 \rangle$ dislocation instead of two $\frac{1}{4}a_0' \langle 111 \rangle$ types. Also, many long, straight faults of the $\langle 100 \rangle$ type were present. The energy of these APB faults is so low that they should not impede the slip of dislocations, so no coupling of their dislocations was observed.

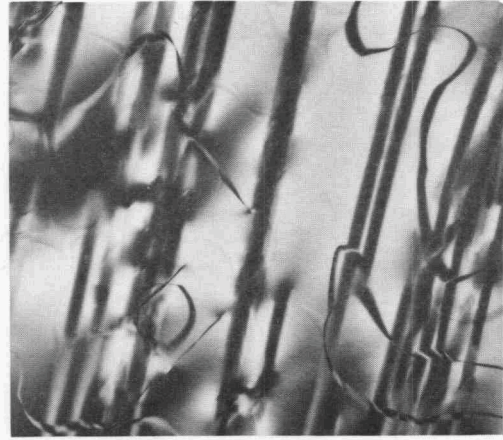
The high yield stress of the 24% Al alloy is caused by the two-phase nature of the material as well as by a low mobility of dislocations coupled loosely with APBs, the glide of which is expected to be subjected to a high lattice frictional stress.¹⁹ Above 26% Al, the APB energy of the $\langle 111 \rangle$ fault vector increases substantially with increasing aluminum content. The continuous drop in yield stress with aluminum concentration above 26% in Fig. 5 is thereby attributed to tightly coupled superlattice dislocations (paired $\frac{1}{4}a_0' \langle 111 \rangle$ type), behaving like single $\frac{1}{2}a_0' \langle 111 \rangle$ dislocations. Our study of dislocation structures and APB types as a function of composition is continuing, and the results of this study will be provided in a separate report.

Figure 8 shows the 0.2% yield strength as a function of temperature for several of the compositions studied. For clarity, only the data for the 24 and 28% Al alloys are included. The curve for the 25% Al alloy was similar to that for the 24%; the curves of the 26, 27, and 30% Al alloys were similar to that of 28%. Other researchers have shown that σ_y near

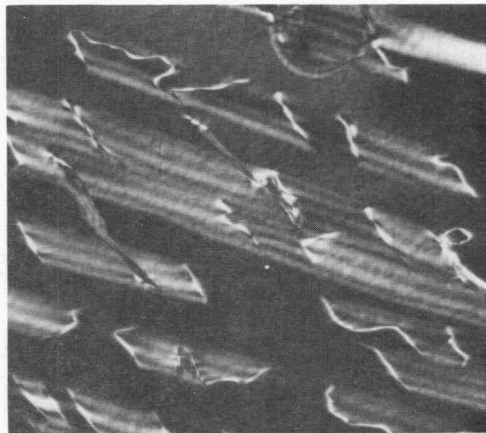
YE13400

(a) $1 \mu\text{m}$

YE13399

(b) $1 \mu\text{m}$

YE13401

(c) $0.5 \mu\text{m}$

YE13402

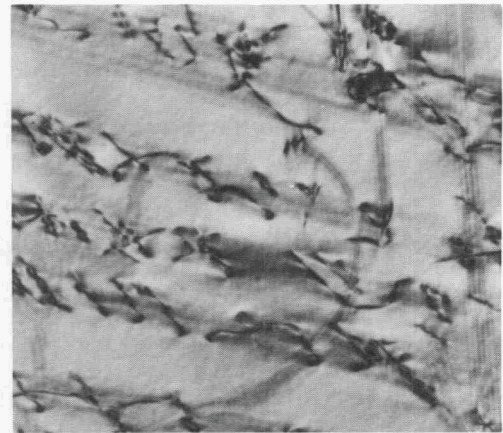
(d) $0.5 \mu\text{m}$

Fig. 7. Transmission electron micrographs of Fe-26% Al. (a) $\langle 111 \rangle$ dark field showing both DO₃ and B2 APBs. (b) $\langle 222 \rangle$ dark field showing only B2 APBs. (c) $\langle 200 \rangle$ dark field showing $\langle 111 \rangle$ faults between dislocations. (d) Bright field showing curved APB ending in a dislocation.

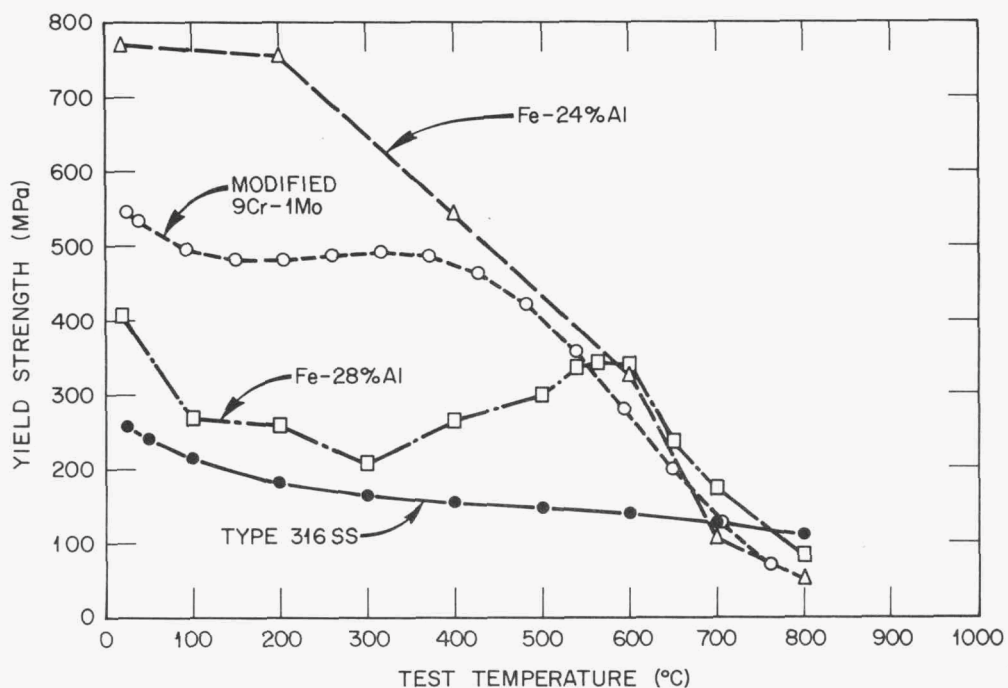


Fig. 8. Yield stress of iron aluminides vs test temperature and comparison to modified 9Cr-1Mo and type 316 SS.

the Fe_3Al composition increases with temperature above 300°C to a maximum value near 550°C and then decreases sharply.^{10,11,13} This temperature corresponds to the second-order phase transformation temperature between the D0_3 and the B2 ordered structures.^{4,6} Morgand et al.¹³ showed that this peak in σ_y occurs clearly at compositions from ~ 23 to $\sim 32\%$ Al, which coincides with the composition range of the D0_3 phase. As noted earlier, this type of yield behavior has been observed in many other ordered systems and several different mechanisms have been proposed to explain its presence as a function of temperature. However, none of the proposed mechanisms appears to be entirely applicable to the Fe_3Al system. It is seen from Fig. 8 that, under the conditions of our test, the alloys containing 24 and 25% Al did not show the same yield behavior as the 26–30% Al alloys. As noted above, Inouye³⁶ reported that alloys of 24 and 25% Al are age-hardenable above 400°C , because of the precipitation of α from the ordered D0_3 phase. The higher yield strength of these alloys at ambient temperatures is a consequence of that age-hardening reaction

produced by our ordering heat treatment of 7 d at 500°C. Inouye also showed that by slow cooling from above 550°C, with no aging, the anomalous yield stress peak could be produced at these compositions. Our data for the 26-30% Al alloys showed the expected anomalous yield behavior with a maximum between 550 and 600°C. This composition range coincides with the presence of the $D0_3$ phase field, as evidenced by the phase diagram (Fig. 1).

Figure 8 also presents a comparison of the yield strength of the iron aluminides near the 28% Al composition with that of type 316 SS and modified 9Cr-1Mo alloy. It can be seen that the yield strength of the iron aluminides is better than that of type 316 SS up to 760°C and better than that of modified 9Cr-1Mo steel above 550°C. However, the ductility at temperatures below 400°C (Fig. 9) needs to be improved.

5. DEVELOPMENT OF ALUMINIDE ALLOYS

The binary alloy Fe-28% Al, with and without TiB_2 , was chosen as the base alloy for further study. Table 2 lists the elements that have been added as alloying agents and the composition ranges that have been used.

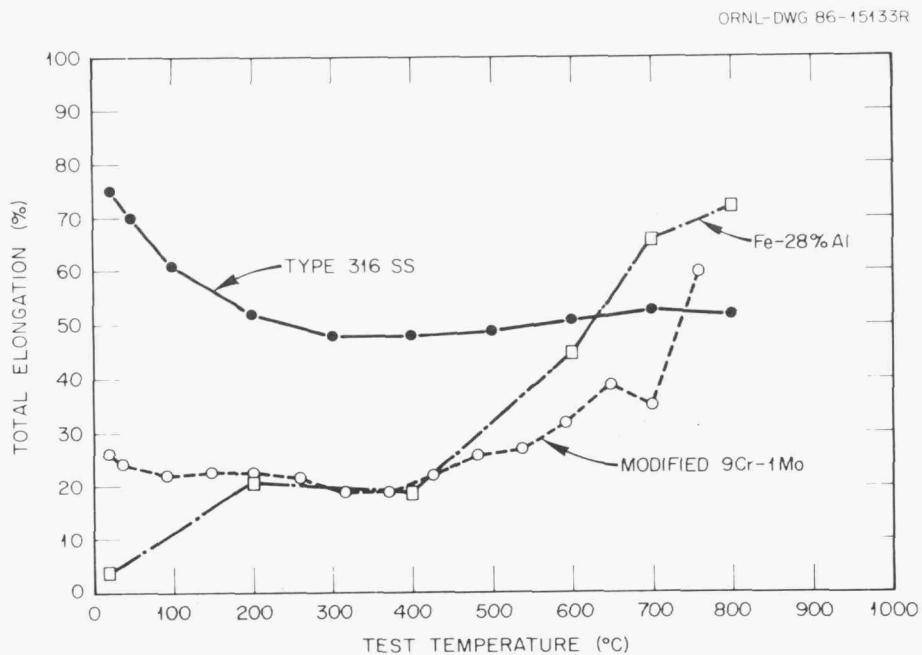


Fig. 9. Ductility vs temperature for Fe-28% Al compared with modified 9Cr-1Mo and type 316 SS.

Table 2. Alloying agents currently being studied

Additive	Amounts added (at. %)	Additive	Amounts added (at. %)
TiB ₂	1	Ti	2
Mo	0.5-2.0	Zr	0.1-2.0
Mn	4-6	B	0.1-0.2
Cr	2-6	Ce	0.01-0.03
Nb	0.5-2.0	Y	0.01-0.03

These elements were added to the Fe-28 % Al base composition singly to produce ternary alloys or in combinations of two or more. Initially, the TiB₂ precipitates were added for grain refinement. However, as will be discussed, these precipitates seemed to cause cracks during welding of the alloys. Because of this cracking problem and because grain refinement could be produced by the addition of certain other elements, the addition of TiB₂ was halted. A total of 45 alloys, listed in Table 3, have been prepared by standard arc-melting, drop-casting, and hot-rolling procedures, as explained above. For the purposes of this report, they have been designated as ternary or multicomponent alloys.

Table 3. Alloys currently being studied

Alloy designation FA-	TiB ₂ added ^a	Alloying element
37, 61	Y, N	Base alloys
52, 53, 56	Y	Mo
62	N	Mo
69, 70	Y	Mn
71	N	Mn
63, 64, 65	Y	Cr
77, 72, 78	N	Cr
59, 66	Y	Nb
79	N	Nb
57, 58	Y	Ce
67, 68	Y	Y
60	Y	B
54	Y	Zr
55	Y	Ti
73-75	N	Combinations of
80-98	N	the above

^aTiB₂ was added to some alloys as precipitates to refine grain size (Y = yes, N = no).

5.1 FABRICABILITY

Specimens for this study were prepared by hot rolling at temperatures from 1000 to 650°C, followed by a final warm rolling at 600°C to produce a cold-worked structure. Only alloy FA-54, containing 2% Zr, experienced difficulty during the rolling procedure. That alloy was very brittle and cracked excessively during rolling at temperatures lower than 800°C. Its microstructure, both as rolled and after a standard heat treatment of 1 h at 850°C plus 7 d at 500°C, showed many large zirconium-based precipitates. A few of the multicomponent alloys experienced some degree of cracking during the final rolling at 600°C. However, the cracking cannot be simply correlated with alloy composition and microstructure.

5.2 MICROSTRUCTURES

Figure 10 shows the as-rolled microstructures of alloys FA-37, -72, -84, and -91, which are typical of those produced in this study. All alloys that contained TiB₂ (except alloy FA-54 with zirconium) exhibited a rolled structure similar to that of FA-37 [Fig. 10(a)] with elongated grains of <50- μ m width. Binary alloys without TiB₂ had somewhat larger elongated grains of up to 150- μ m width, as shown by FA-72 [Fig. 10(b)]. All the multicomponent alloys, except FA-84, -85, and -86, exhibited grains of ~10-30- μ m width [Fig. 10(c)], probably due to the precipitates produced by alloying. Alloys FA-84, -85, and -86 had grains of up to 50- μ m width and showed fewer precipitates than the other multicomponent alloys [Fig. 10(d)].

The microstructures of all alloys were studied after the standard anneal of 1 h at 850°C (for recrystallization) and 7 d at 500°C (for producing the DO₃ ordered structure). In the following discussion, the ternary alloys (with and without TiB₂) and the multicomponent alloys will be considered separately.

5.2.1 Ternary Alloys

Figures 11 and 12 show recrystallized microstructures for several of the alloys studied. The alloys in Fig. 11(a)-(c) and in Fig. 12 contain TiB₂ and had grain sizes of no larger than ~60 μ m (Table 4). Additions of molybdenum, niobium, titanium, boron, and zirconium reduced the grain

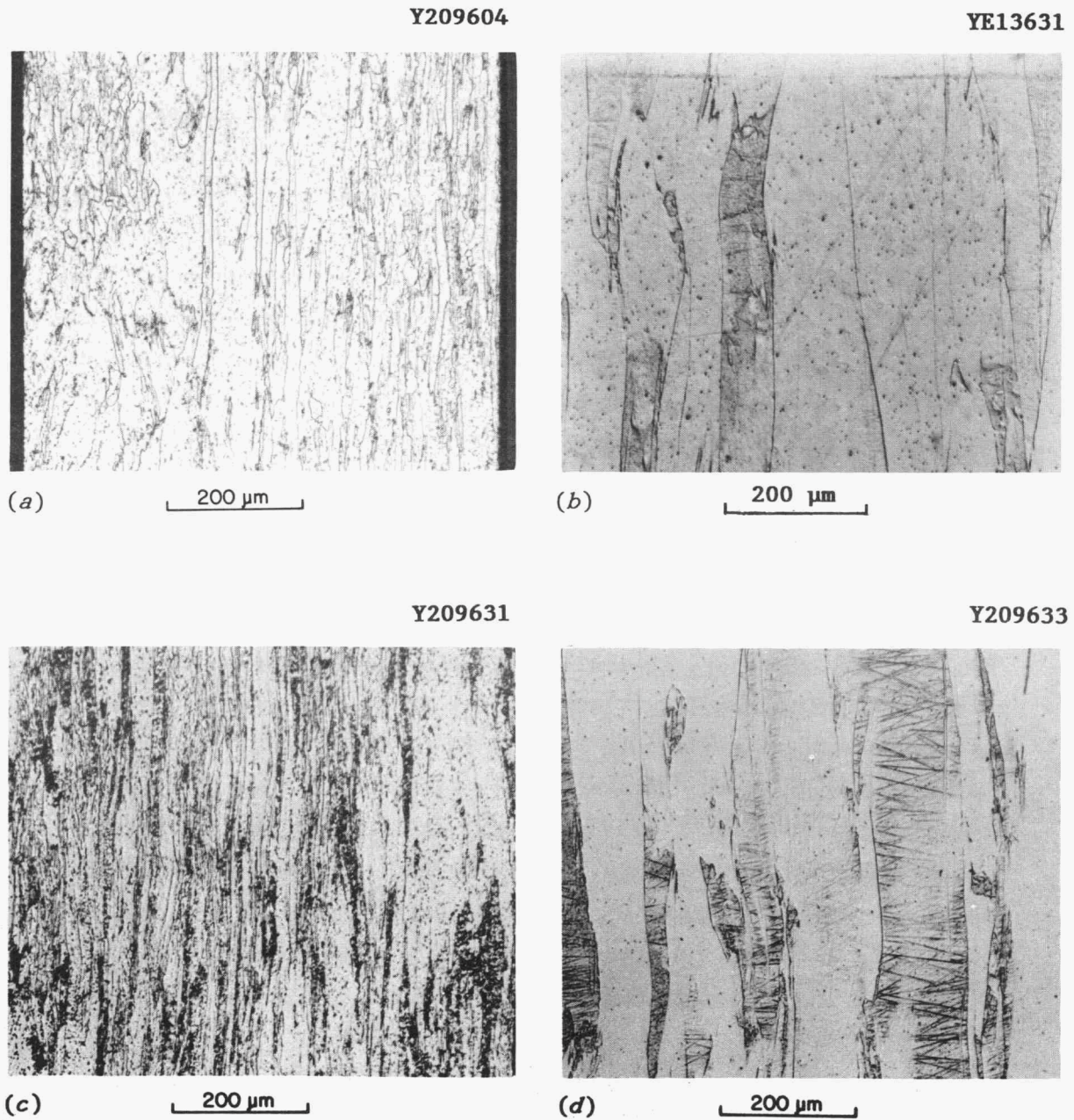


Fig. 10. As-rolled microstructures of several iron-aluminum alloys. (a) FA-37 base alloy, (b) FA-72, (c) FA-91, and (d) FA-84. All micrographs are 100X.

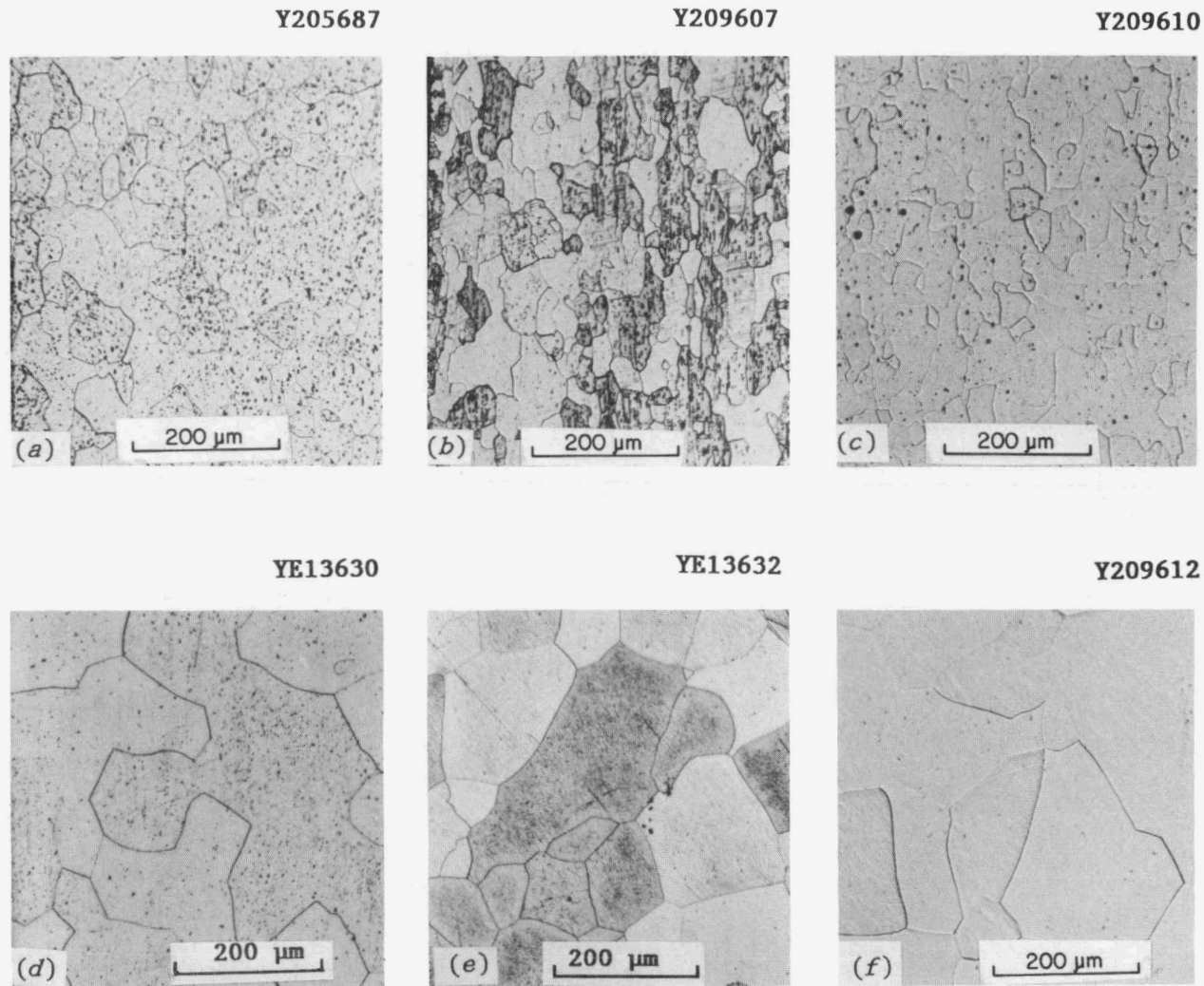


Fig. 11. Microstructures of binary and ternary alloys with and without TiB_2 after recrystallization at $850^\circ C$ and an ordering heat treatment at $500^\circ C$. (a) Base alloy FA-37, Fe-28% Al with TiB_2 . (b) FA-64, with 4% Cr and TiB_2 . (c) FA-69, with 4% Mn and TiB_2 . (d) FA-61, base alloy without TiB_2 . (e) FA-72, with 4% Cr and no TiB_2 . (f) FA-71, with 4% Mn and no TiB_2 . All micrographs are 100X.

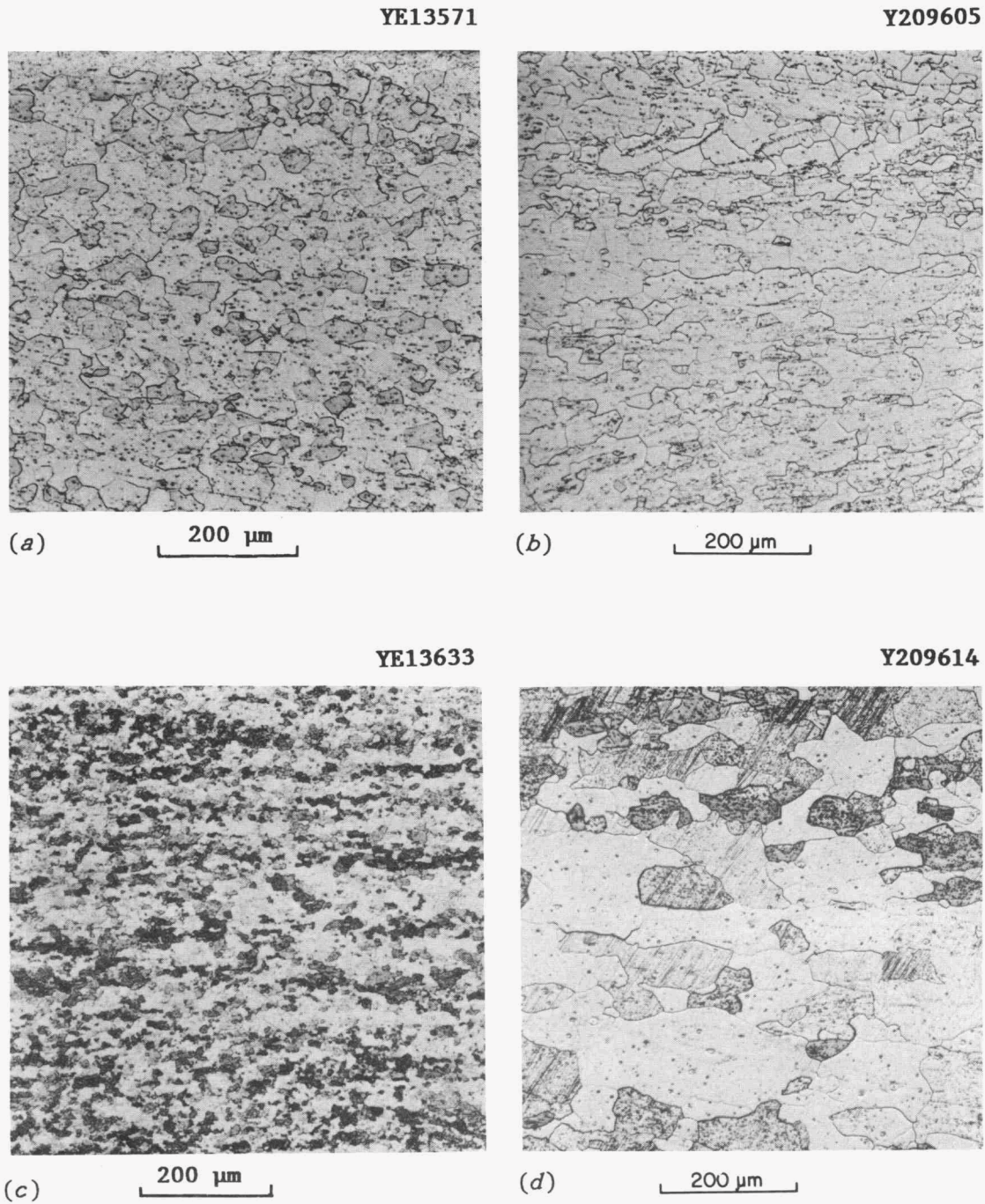


Fig. 12. Microstructures of several ternary alloys (all with TiB_2) after recrystallization at $850^\circ C$ and an ordering heat treatment at $500^\circ C$. (a) FA-56, with 2% Mo. (b) FA-59, with 1% Nb. (c) FA-54, with 2% Zr. (d) FA-58, with 0.03% Ce. All micrographs are 100X.

Table 4. Effect of alloying additions on grain size of Fe₃Al with and without TiB₂

Alloy addition (at. %)	With TiB ₂		Without TiB ₂	
	Alloy designation FA-	Grain size (μm)	Alloy designation FA-	Grain size (μm)
Base	37	50	61	118
Mo				
0.5	52	25		
1.0	53	25		
2.0	56	25	62	87
Nb				
1.0	59	30	79	65 ^a
2.0	66	15		
Mn				
4.0	69	50	71	167
6.0	70	40		
Cr				
2.0	63	60	77	105
4.0	64	50	72	112
6.0	65	50	78	129
Ti			<i>c</i>	
2.0	55	30		
Ce			<i>c</i>	
0.01	57	50		
0.03	58	50		
Y			<i>c</i>	
0.01	67	50		
0.03	68	50		
B			<i>c</i>	
1.0	60	25		
Zr			<i>c</i>	
2.0	54	30 ^b		

^aAll values in this table are from samples recrystallized at 850°C, except FA-79 which had not recrystallized at that temperature. Instead, a temperature of 950°C was used.

^bApproximate value. The great number of precipitates prevented an accurate measurement.

^cNo alloys with this element were prepared without TiB₂.

size when compared with the 50- μm grain size of the base alloy, while additions of chromium, manganese, cerium, and yttrium did not seem to have much effect. Additions of cerium, yttrium, boron, manganese, zirconium, and molybdenum appeared to coarsen the precipitates already present. Whether they also added more precipitates will require more study. Most elements were added in more than one concentration, but only one element exhibited an effect on grain size with increased addition. That element, niobium, produced grain sizes of 50, 30, and 15 μm with additions of 0, 1, and 2%, respectively.

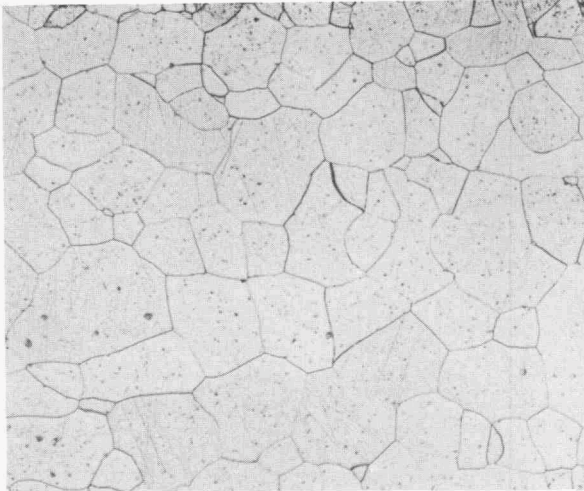
The micrographs in Fig. 11(d)-(f) show the base alloy and ternary alloys containing 4% Cr and 4% Mn without TiB_2 , respectively. From Fig. 11 and Table 4 it is seen that the addition of TiB_2 produced a decrease in grain size of two to three times. Table 4 also indicates a small reverse effect on grain size with the addition of chromium; 105, 112, and 129 μm for additions of 2, 4, and 6% Cr, respectively.

5.2.2 Multicomponent Alloys

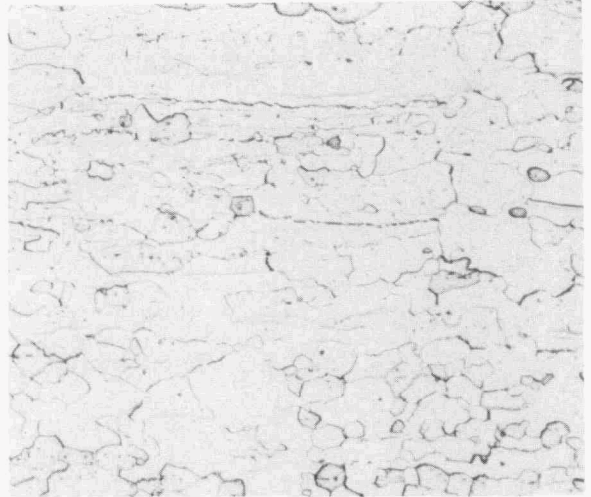
From the results of our earlier studies on the ternary series of alloys, we have chosen chromium, molybdenum, and niobium as important elements for improving room-temperature ductility, creep resistance, and high-temperature strength. Therefore, the microstructures of the multicomponent alloys under study, presented in Figs. 13 through 17, have been divided according to the major alloying elements: Fig. 13 contains alloys whose major addition is chromium; Fig. 14, molybdenum; Fig. 15, chromium and niobium; Fig. 16, chromium and molybdenum; and Fig. 17, chromium, molybdenum, and niobium. Again, all these alloys were heat treated as described above.

Figure 13 presents alloys of Fe-28% Al with chromium and small amounts of boron, yttrium, and/or zirconium. Boron, in the levels studied here, appears to go into solution unless another element such as zirconium is present, which tends to form borides. With or without TiB_2 , zirconium forms precipitates even at the 0.1% level. As noted above for niobium with and without TiB_2 , the addition of small amounts of zirconium results in an increase in the recrystallization temperature [note the partially

Y209629

(a) 200 μ m

Y209627

(b) 200 μ m

Y209626

(c) 200 μ m

Y209622

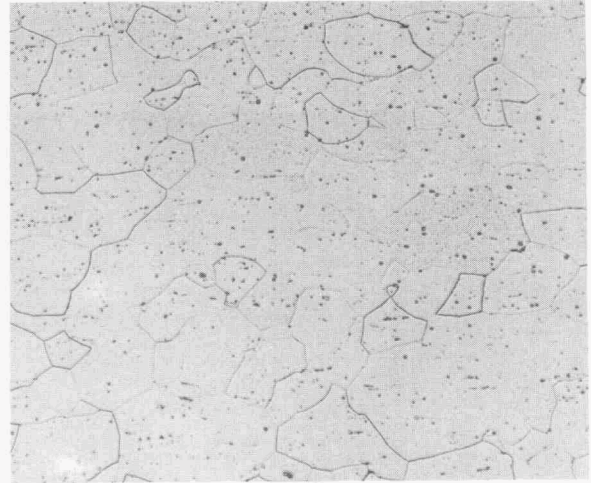
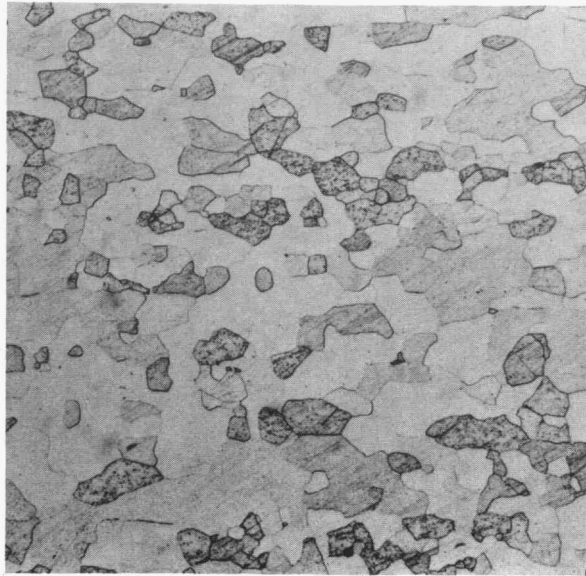
(d) 200 μ m

Fig. 13. Microstructures of several multicomponent alloys with chromium as the major alloying addition, after recrystallization at 850°C and an ordering heat treatment at 500°C. (a) FA-84. (b) FA-89. (c) FA-90. (d) FA-98. All micrographs are 100X.

YE13634

Y209624



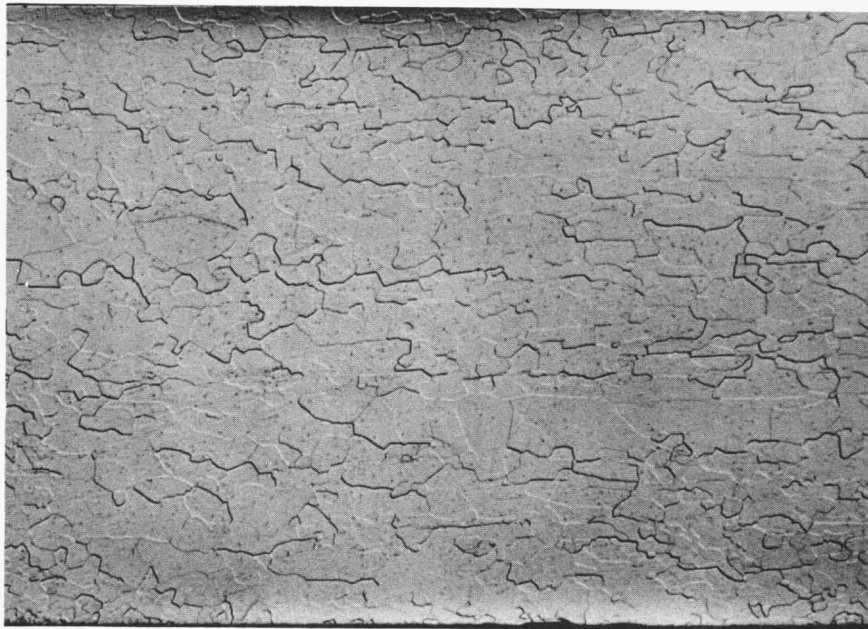
(a)

200 μm 

(b)

200 μm

Y209617

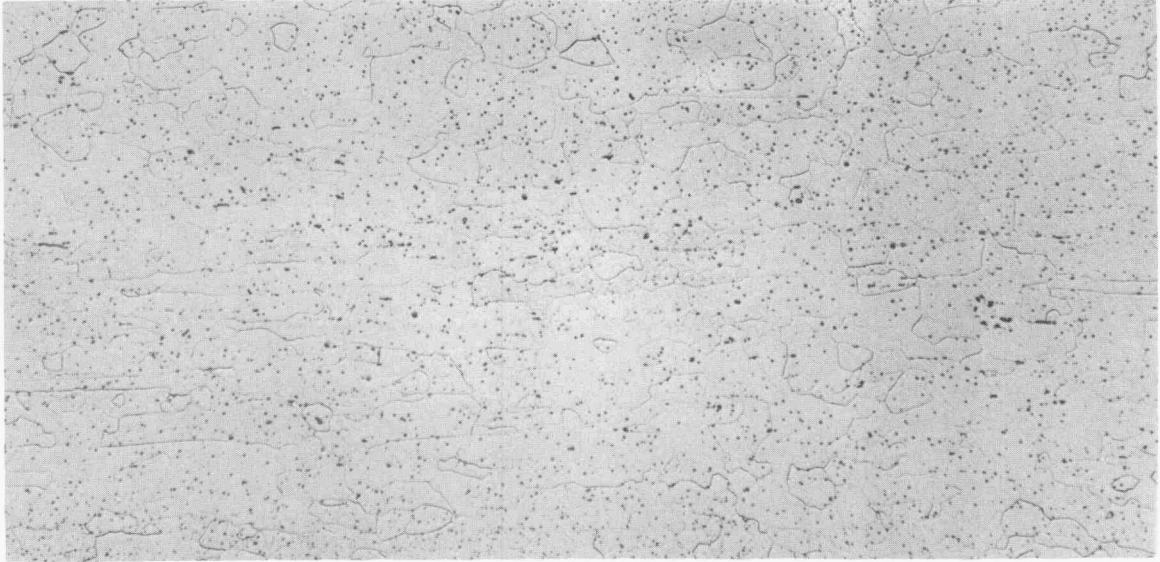


(c)

200 μm

Fig. 14. Microstructures of multicomponent alloys with molybdenum as the major alloying addition, after recrystallization at 850°C and an ordering heat treatment at 500°C. (a) FA-73. (b) FA-91. (c) FA-92. All micrographs are 100X.

Y209615



(a)

200 μm

Y209618



(b)

200 μm

Fig. 15. Microstructures of multicomponent alloys with chromium and niobium as the major alloying additions, after recrystallization at 850°C and an ordering heat treatment at 500°C. (a) FA-81. (b) FA-93. All micrographs are 100X.

YE13637



(a)

200 μm

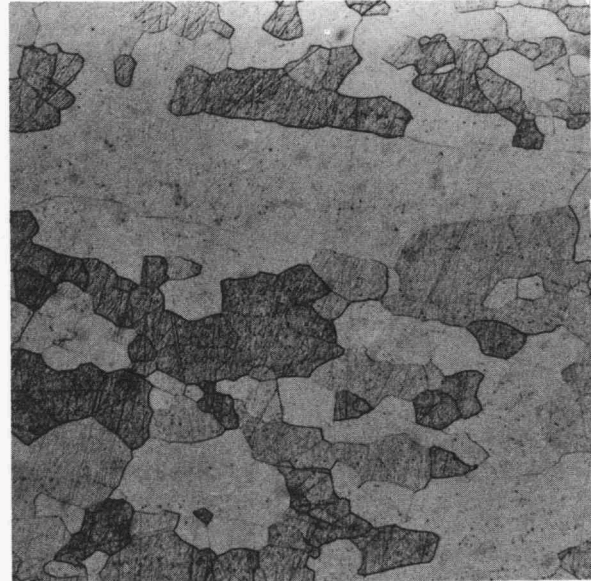
Y209619



(b)

200 μm

YE13636



(c)

200 μm

Fig. 16. Microstructures of multicomponent alloys with chromium and molybdenum as the major alloying additions, after recrystallization at 850°C and an ordering heat treatment at 500°C. (a) FA-85. (b) FA-95. (c) FA-86. All micrographs are 100X.

Y209620



(a)

200 μm

Y209621



(b)

200 μm

Fig. 17. Microstructures of multicomponent alloys with chromium, molybdenum, and niobium as the major alloying additions, after recrystallization at 850°C and an ordering heat treatment at 500°C. (a) FA-96. (b) FA-97. All micrographs are 100X.

recrystallized microstructure in Fig. 13(c)] unless boron is also present, in which case the grain size is refined but recrystallization is complete [Fig. 13(d)].

Figure 14 shows alloys with molybdenum and small amounts of boron and/or zirconium. All three alloys contain precipitates because molybdenum appears to form precipitates easily when boron is present. However, the alloy with only zirconium added Fig. 14(b) contains much coarser precipitates than those that also contain boron. Although molybdenum increased the recrystallization temperature,⁴⁰ this figure and other figures in this series indicate that even small amounts of zirconium can also increase the recrystallization temperature in these alloys.

The two alloys shown in Fig. 15 contain the same amounts of chromium and niobium, but only 26% Al and small amounts of either boron [Fig. 15(a)] or zirconium [Fig. 15(b)]. Both alloys appear to be less than 100% recrystallized. The smaller average grain size of the alloy containing zirconium is also noted.

Figures 16 and 17 show the microstructures of alloys containing chromium and molybdenum and alloys containing chromium, molybdenum, and niobium, respectively, with small additions of boron and/or zirconium. The effect of zirconium on recrystallization temperature, grain size, and the presence of precipitates, as discussed above for Figs. 13 to 14, is noted.

All these results suggest that the formation of fine, second-phase particles (e.g., TiB_2 , zirconium, or niobium precipitates) is more effective in refining grain size and increasing the recrystallization temperature than is alloying with elements that form solid solutions. This conclusion was also reached by Mendiratta et al.,⁴¹ who found that the addition of 1-2% zirconium or niobium produced second-phase particles that seemed to strengthen Fe_3Al at higher temperatures.

5.3 TENSILE PROPERTIES

5.3.1 Ternary Alloys

Figures 18 and 19 show the room-temperature yield strength and ductility for the ternary iron-aluminum alloys tested. The alloy designated FA-37 is the base alloy of Fe-28% Al with 1% TiB_2 (0.5 wt %). Compared with this alloy, improvements in room-temperature yield strength

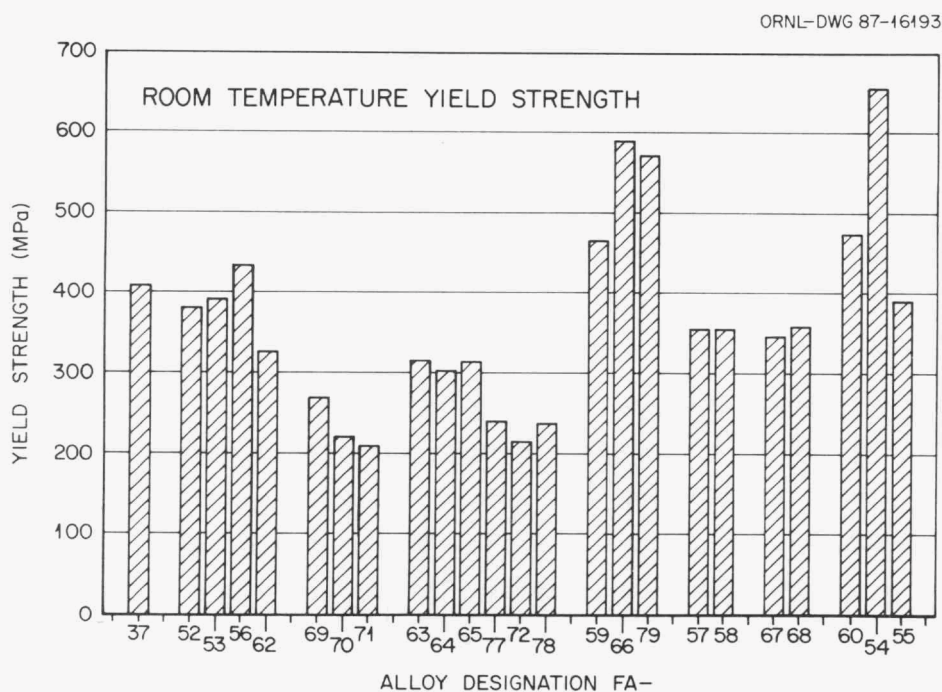


Fig. 18. Room-temperature yield strength of the base alloy FA-37 and ternary iron aluminides, with and without TiB_2 .

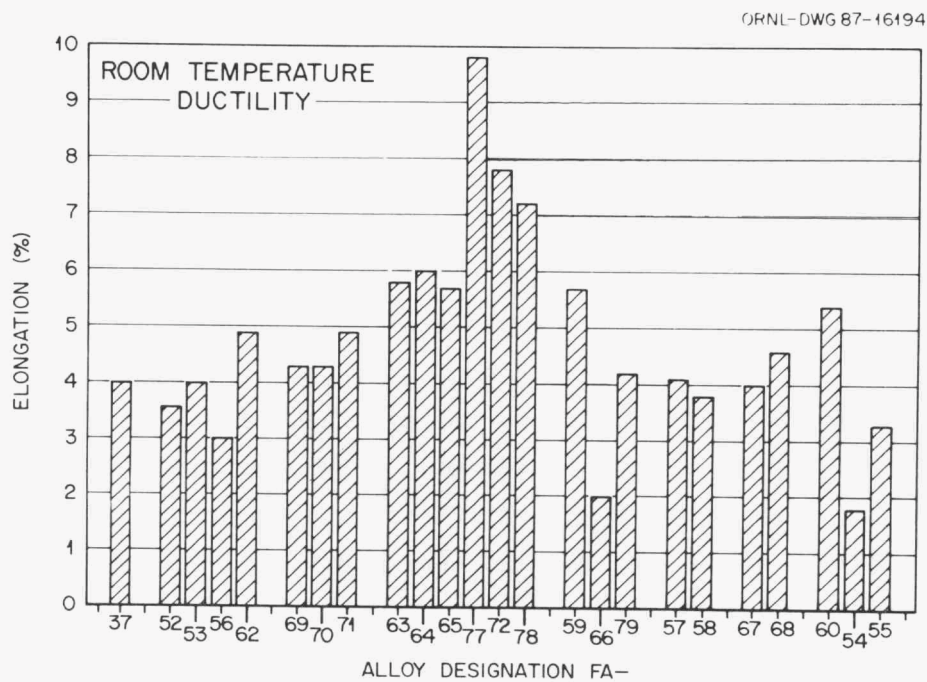


Fig. 19. Room-temperature ductility of the base alloy FA-37 and ternary iron aluminides, with and without TiB_2 .

were seen in alloys FA-56, -59, -66, -79, -60, and -54. Alloys FA-66, -79, and -54 reached yield strengths of above 550 MPa, making them comparable or stronger than modified 9Cr-1Mo alloy. In terms of room-temperature ductility, only alloys FA-77, -72, and -78 containing chromium showed real promise, reaching elongations of more than 7%. With a different heat-treating condition, the elongations of alloys FA-77 and -72 were recently increased to above 10%. Several other alloys had elongations greater than the base alloy, but the slight improvement they produced was not deemed adequate for further study.

Figure 20 shows the yield strength for alloys tested at 600°C. Values in excess of 300 MPa were seen for all alloys tested, with a maximum of 516 MPa for an alloy containing TiB_2 and niobium (FA-66). These strengths are much higher than either the modified 9Cr-1Mo alloy or type 316 SS. Elongations at this temperature were in excess of 30% for all alloys tested, except FA-62 which was 15%.

From these results, it was determined that chromium is needed for better room-temperature ductility. This element may modify slip behavior and/or enhance grain boundary cohesive strength, resulting in improved room-temperature ductility. Detailed microstructural analysis is needed to characterize its beneficial effects. The elements niobium and molybdenum improve the strength, especially at higher temperatures.

5.3.2 Multicomponent Alloys

Room-temperature tensile properties of the multicomponent alloys are presented in Figs. 21 and 22. Only alloys FA-80, -81, and -82 have higher yield strengths than the base alloy. However, all the alloys charted in Fig. 21 have higher or comparable yield strengths when compared to type 316 SS. The room-temperature ductility has not been further improved by alloying with multiple elements. Alloys FA-81 and -83, which contain chromium as one of the alloying elements, produced elongations of ~9% (Fig. 22), compared with almost 10% for the ternary alloys containing chromium. Alloys FA-90 and -73 also show promise for giving some improvement in ductility.

Figure 23 shows the yield strength at 600°C of the multicomponent alloys. All alloys had yield strengths greater than type 316 SS at this temperature. Elongations were in excess of 20%.

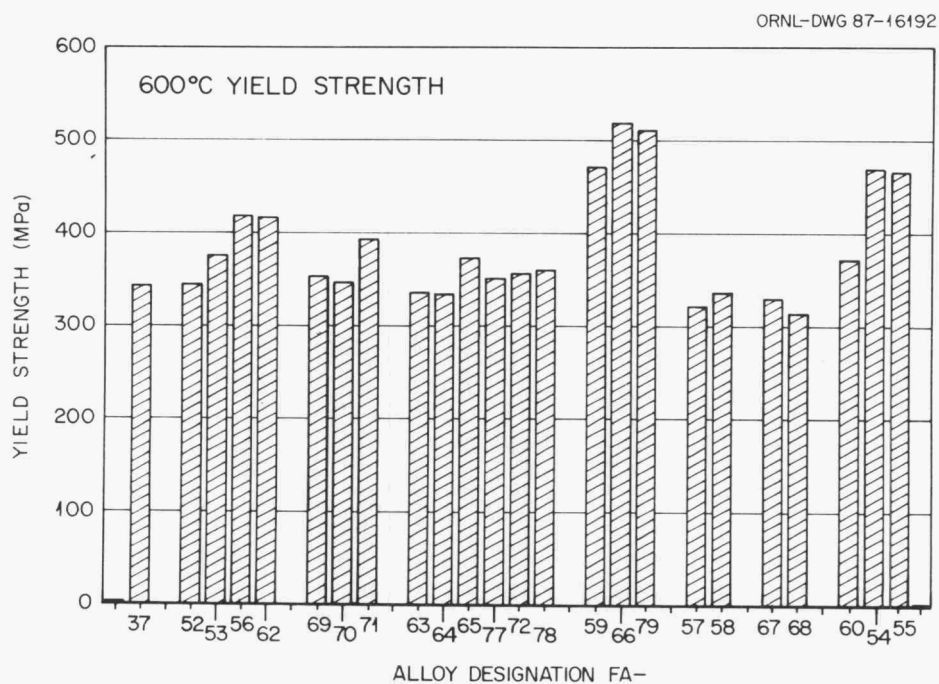


Fig. 20. Yield strength at 600°C of the base alloy FA-37 and ternary iron aluminides, with and without TiB₂.

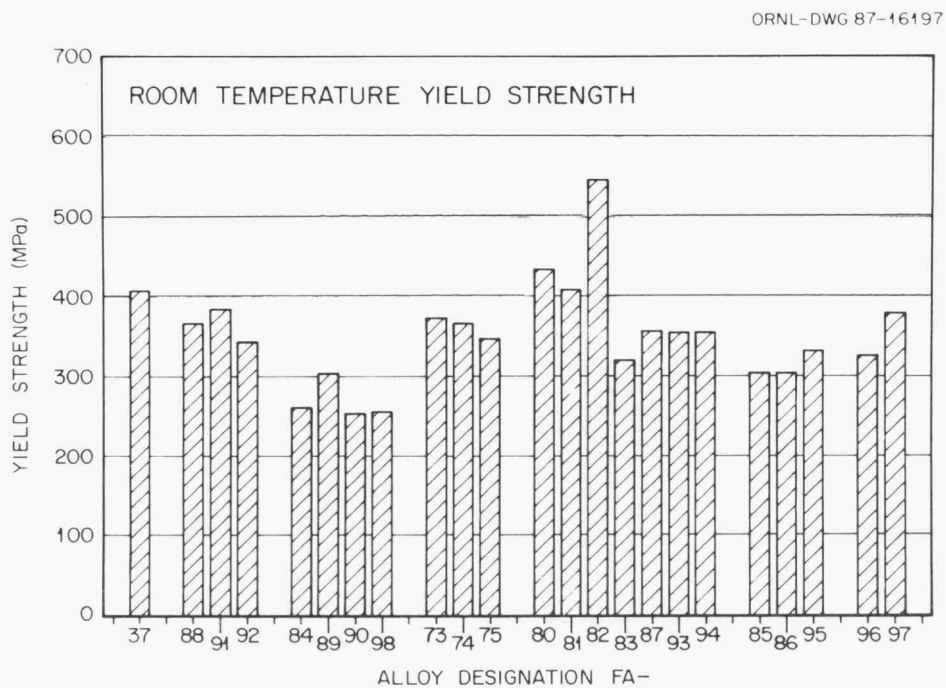


Fig. 21. Room-temperature yield strength of the base alloy FA-37 and multicomponent alloys.

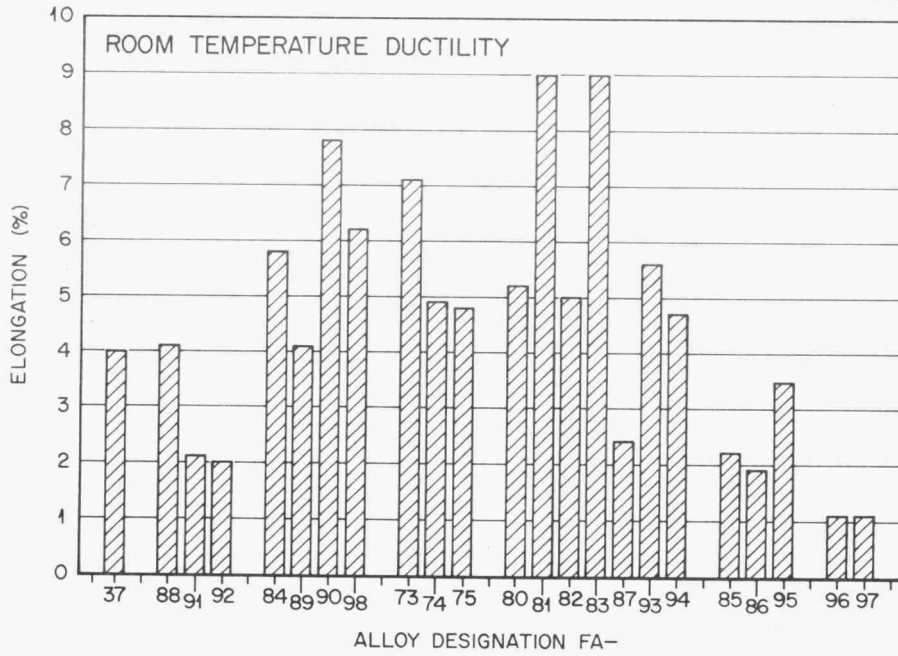


Fig. 22. Room-temperature ductility of the base alloy FA-37 and multicomponent alloys.

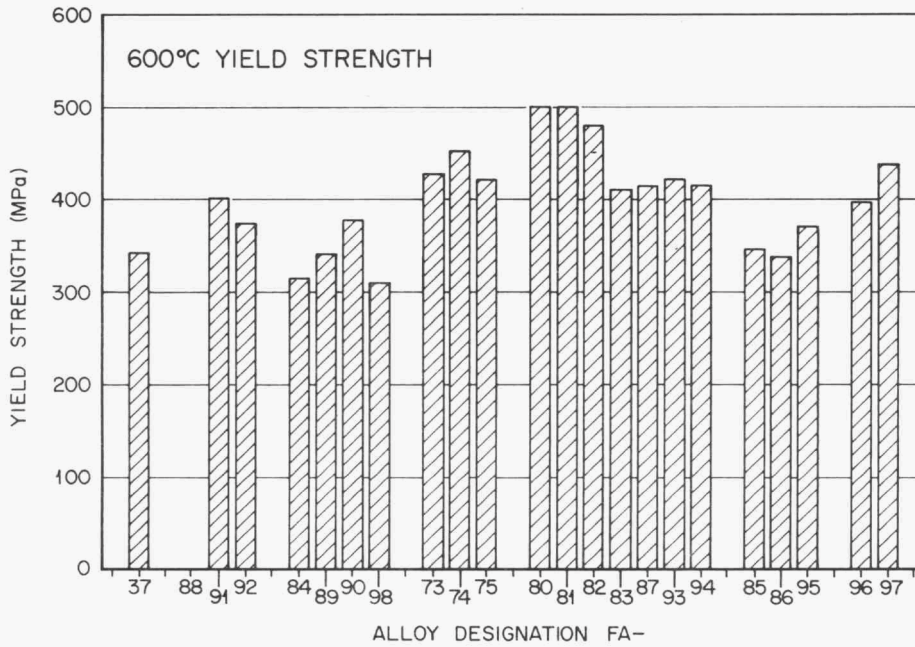


Fig. 23. Yield strength at 600°C of the base alloy FA-37 and multicomponent alloys.

5.4 FRACTURE SURFACES

The fracture surfaces of most of the alloys studied are characterized by a mixed intergranular-transgranular cleavage mode of failure, as shown in Fig. 24(a) and (b). These fractographs, showing the tensile fracture surfaces of FA-37 (base alloy) and FA-56 (2% Mo), show numerous TiB_2 precipitates and many cracks along the grain boundaries. The same alloys, without TiB_2 , showed almost completely transgranular cleavage, in agreement with Horton et al.²⁸ [Fig. 24(c) and (d)]. All alloys containing TiB_2 precipitates had the same mixed-mode fracture surface as alloys FA-37 and -56, except alloy FA-60 (Fig. 25) which contained excess boron. The addition of boron to binary alloys containing TiB_2 appears to facilitate a change in fracture mode from intergranular to transgranular cleavage. Also, comparison of the tensile properties of FA-37 and -62 vs FA-60 and -73 (in the last section of this report) shows a slight improvement with the addition of boron. This effect certainly requires more study.

The fracture surfaces of the multicomponent alloys were characterized by smaller grains, many precipitates, and more transgranular cleavage than the ternary alloys. Alloys containing zirconium seemed to contain the highest number of precipitates, as seen in Fig. 26 for alloy FA-94. All but one of the multicomponent alloys contained zirconium and/or boron.

5.5 CREEP PROPERTIES

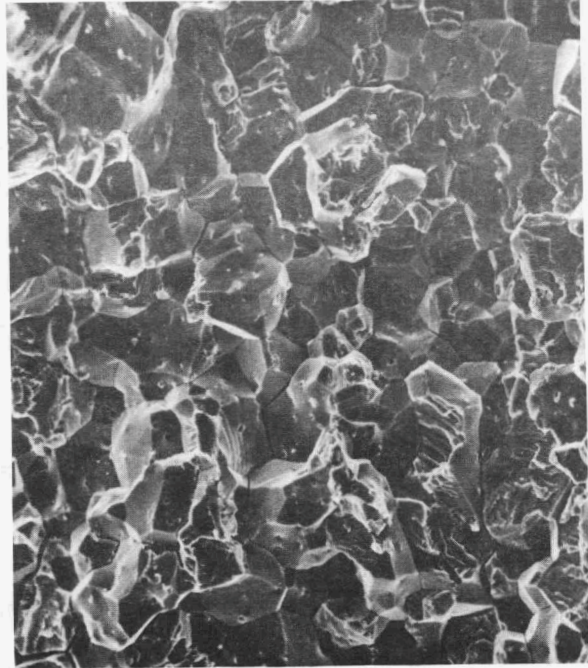
Table 5 summarizes the creep results obtained for several alloys after a heat treatment of 1 h at 850°C plus 7 d at 500°C. The base alloy FA-61 (Fe-28% Al, no TiB_2) is weak in creep resistance. The creep properties of the iron aluminides can be improved by alloying with chromium, niobium, and molybdenum. Although niobium is most effective in increasing tensile strength at elevated temperatures, Table 5 indicates that molybdenum is most beneficial in improving creep resistance. The creep properties of FA-73, containing molybdenum, are comparable to type 304 austenitic SS at the same test condition. Alloys FA-91 and -92 also contain molybdenum and exhibited creep resistance comparable to many stainless steel and nickel-based alloys. All the alloys showed excellent ductilities (>20%) in creep. No substantial difference in creep resistance was noted for specimens in the as-wrought condition.

YE13576



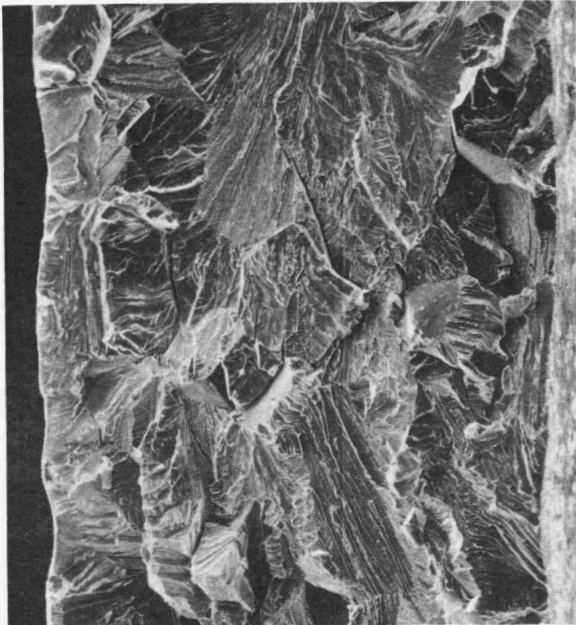
(a)

YE13574



(b)

YE13578



(c)

YE13575



(d)

Fig. 24. Fracture surfaces of several alloys tested in tension. (a) FA-37, 500X. (b) FA-56, 500X. (c) FA-61, 100X. (d) FA-62, 100X.

YE13629

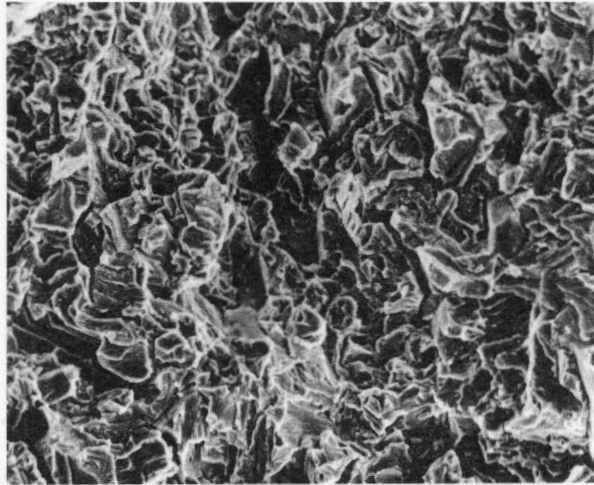
20 μm

Fig. 25. Fracture surface in tension of FA-60 containing TiB_2 and extra boron showing the effect of boron on the fracture mode of the base alloy. Compare with Fig. 24(a). 500X.

YE13628

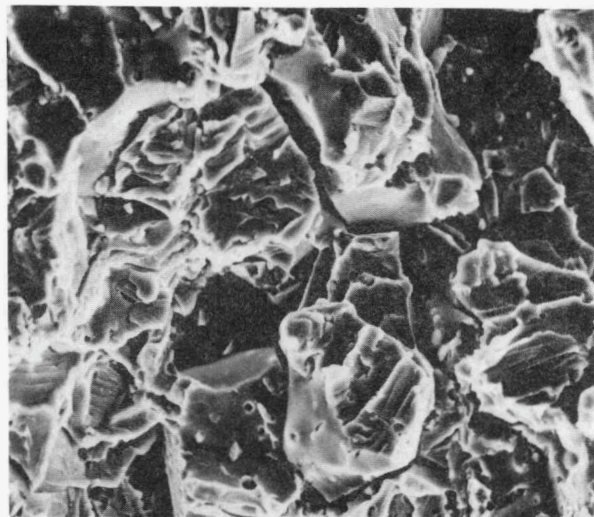
10 μm

Fig. 26. Fracture surface in tension of FA-94 (containing no TiB_2) showing numerous precipitates. 1000X.

Table 5. Creep properties of iron aluminide alloys^a

Alloy designation FA-	Major alloying element	Rupture life (h)	Creep ductility (%)
61		1.6	33.6
77	Cr	3.6	29.2
81	Cr	18.8	64.5
73	Mo	57.4	24.9
88	Mo	15.9	45.0
91	Mo	204.2	20.6
92	Mo	128.1	66.7

^aTested at 207 MPa (30 ksi) and 593°C in air.

5.6 OXIDATION RESISTANCE

Preliminary oxidation tests have been conducted on alloys FA-72, -77, -78, -79, -81, and -83. These alloys were tested in air at temperatures of 800 and 1000°C, with periodic weight measurements being used as a measure of the oxidation resistance. After 500 h at 800°C, all alloys showed excellent resistance to oxidation, with weight gains of <1 mg/cm². The data for alloys FA-78, -79, and -81 are presented in Fig. 27, along with the data collected previously for alloy FA-41 (Fe-27% Al) and type 316 SS. Our tests at 1000°C indicate that oxidation resistance may be just as good at this higher temperature; all alloys studied showed weight changes of less than 4 mg/cm². At both temperatures, alloy FA-81 appears to exhibit the best oxidation resistance (<1 mg/cm² weight change at both 800 and 1000°C).

Several of our original binary alloys (Fe-24 to 30% Al) plus the ternary alloys FA-72, -77, and -78 are currently being tested statically in distilled water. These samples were given a recrystallization heat treatment of 1 h at 800°C, followed by polishing with 320-grit emery paper to remove any surface flaws. To date, the binary alloys have survived one year without measurable weight gain (weight changes are measurable to ±0.00005 g) and still show the original shiny polished surface. The ternary alloys being tested in this manner have also shown no weight change and remain shiny after approximately nine months.

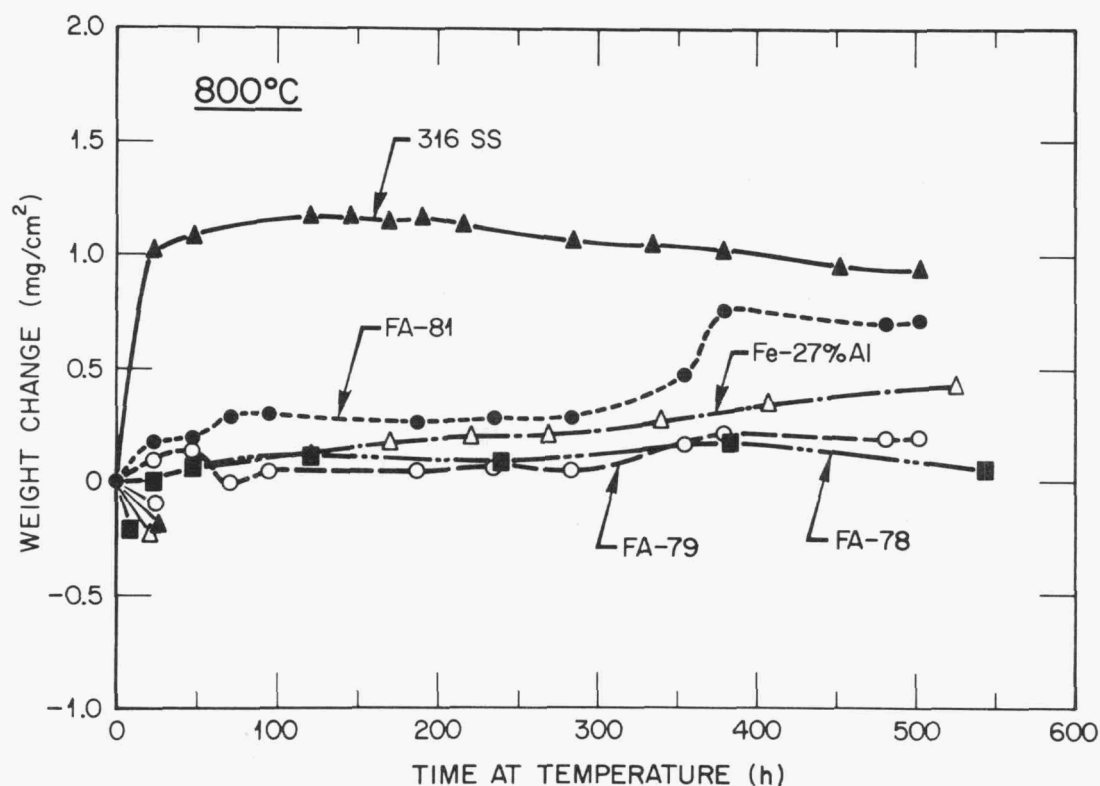


Fig. 27. Oxidation resistance of several iron-aluminum-based alloys at 800°C and comparison with type 316 SS.

5.7 WELDABILITY

Table 6 lists some of the alloys whose weldability have been studied. Welds were made on 0.8-mm-thick, 5- by 5-cm coupons, with speeds of 25.4 to 100 cm/min. Tests of several of the Fe-Al binary alloys (alloys FA-36 through 41) using both EB and GTA welding techniques indicated that the TiB₂ dispersion, which was originally added for grain refinement, is deleterious to the weldability, producing hot cracks along the fusion line (Fig. 28). Most of the ternary and quaternary alloys tested also experienced cracking when TiB₂ was present, but no cracking otherwise. Note that FA-66 containing niobium and TiB₂ showed no cracks during both EB and GTA welding, indicating that niobium is beneficial to the weldability of iron aluminides, even in the presence of TiB₂. Successful

Table 6. Weldability of iron aluminides

Alloy designation FA-	Weldability ^a	
	EB	GTA
39	C	C
41	C	C
61	NC	NC
64	NC	C
66	NC	NC
69	NC	C
72	NC	NC
79	NC	NC
83	NC	NC

^aEB = Electron beam.

GTA = Gas tungsten arc.

C = Cracked.

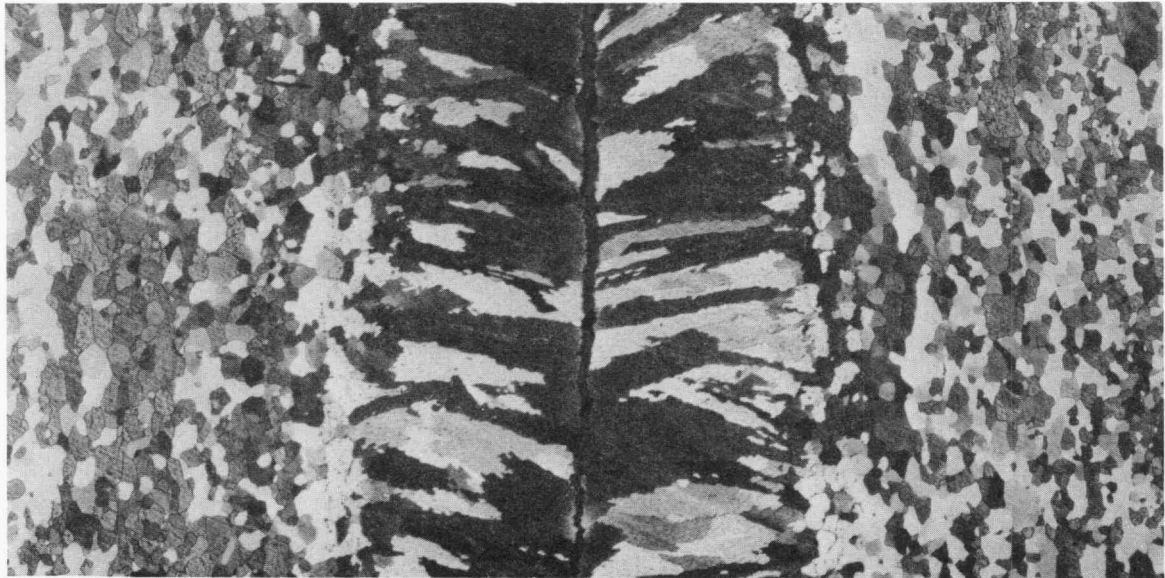
NC = No cracking.

welds without any cracking or other defects were produced in alloy FA-83. Unlike some of the previous alloys, the fusion-zone grain structure of this alloy was very fine. Typical surface and transverse microstructures of the EB weld made at 25.4 cm/min are shown in Fig. 29(a) and (b). Further evaluation of the weldability is under way, but these limited results indicate that iron aluminides near Fe₃Al are basically weldable.

6. SUMMARY

The results of phase 1 indicated that alloys of 24 to 30% Al with small additions of TiB₂ could be fabricated by routine, low-cost melting, casting, and rolling procedures. A self-protecting oxide layer, which forms at low oxygen pressures, provides excellent oxidation and sulfidation resistance. The tensile strengths are higher than those for type 316 SS at temperatures below 760°C and for modified 9Cr-1Mo steel at temperatures above 550°C. The ductility increases with increasing aluminum concentration within this composition range. Our preliminary weldability

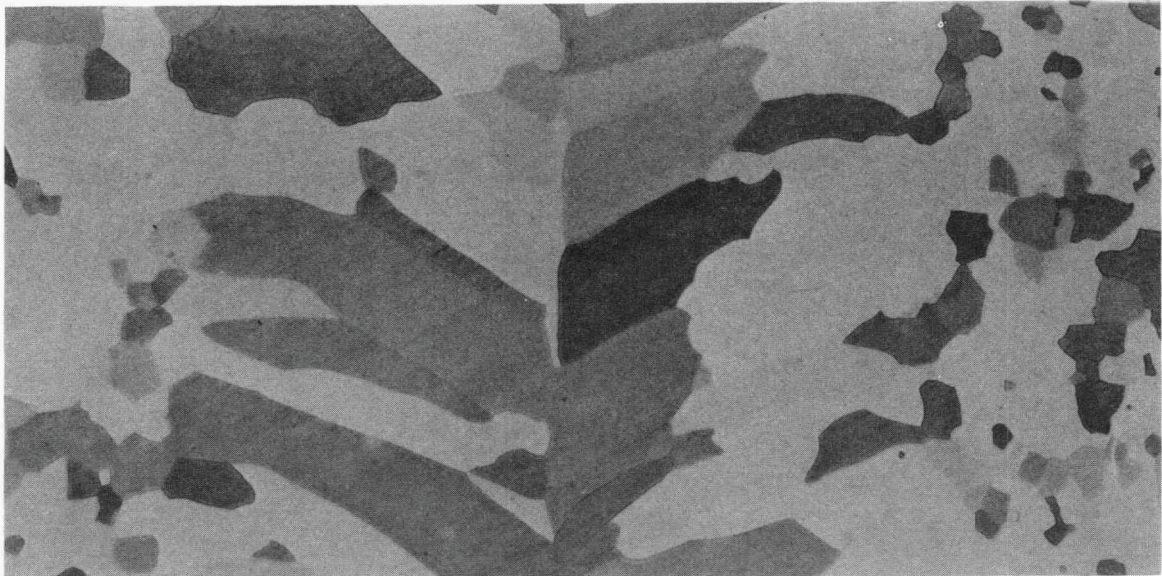
Y206431



(a)

700 μm

Y207163

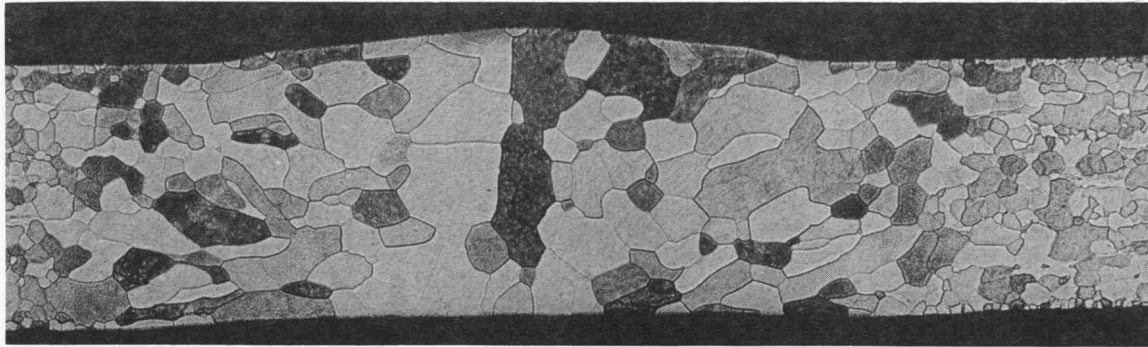


(b)

700 μm

Fig. 28. The effect of the addition of TiB_2 on the electron-beam weldability of Fe-28% Al. (a) Hot cracking along the fusion line with addition of TiB_2 . (b) No cracking when TiB_2 is absent.

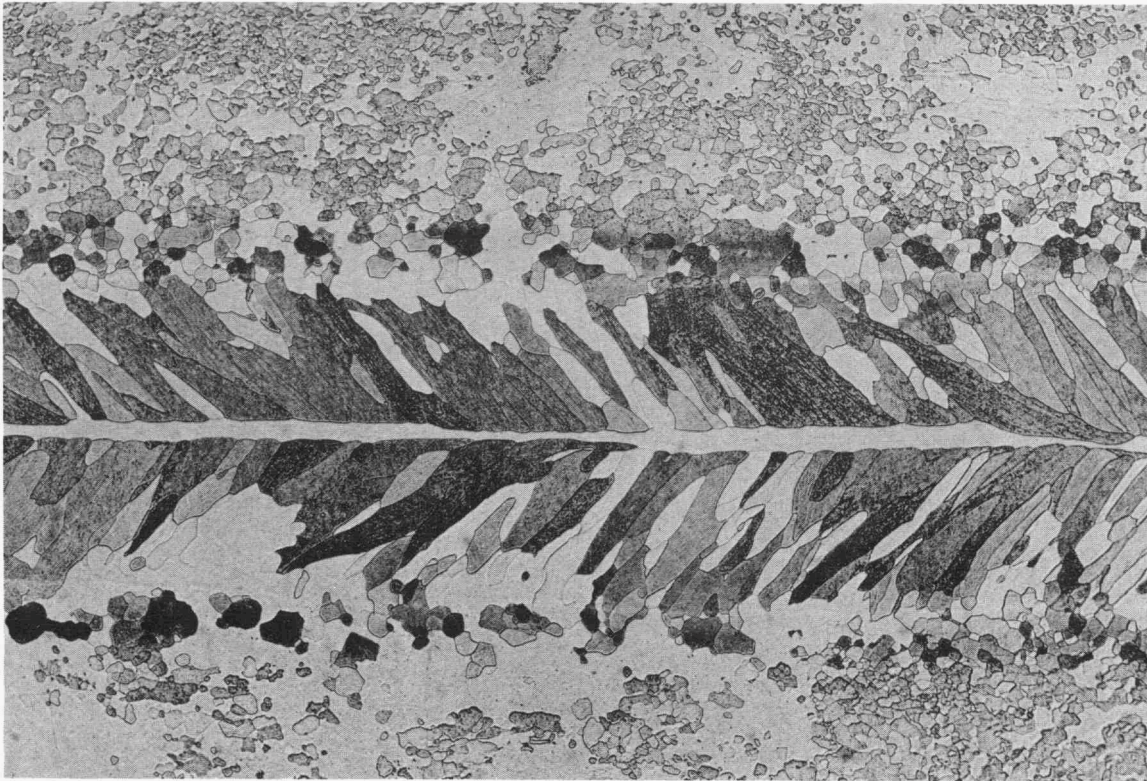
Y208404



(a)

400 μm

Y208403



(b)

800 μm

Fig. 29. (a) Typical surface and (b) transverse microstructures of the electron-beam weld in FA-83 made at 25.4 cm/min.

studies indicate that the alloys with higher aluminum content have fewer cracks in the fusion and heat-affected zones. On the basis of considerations of fabricability, strength, ductility, corrosion resistance, and weldability, the Fe-28% Al alloy was chosen as the base alloy for further development.

It has been shown that, for iron aluminides containing 24-30% Al, the yield strength increases with temperature above 300°C, reaching a maximum at ~550-600°C. This peak is characteristic of Fe₃Al alloys, and the reasons for its occurrence are not fully understood. The presence of the yield stress maximum can be obscured by precipitation reactions at compositions of 24-25% Al and by effects of grain size (such as were noted for an alloy of 35% Al).^{20,38} It was noted that 24-26% Al composition is the range where the dislocation mode changes from the glide of single $\frac{1}{2}a_0 \langle 111 \rangle$ dislocations associated with the α phase to the glide of $\frac{1}{2}a_0 \langle 111 \rangle$ pairs in the DO₃ superlattice. The occurrence of the room-temperature yield stress peak with increasing aluminum concentration is due to precipitation hardening and low mobility of either single dislocations or paired superlattice dislocations at compositions below 26% Al. Alloys of 26% Al and above, which are single-phase DO₃ and therefore do not precipitation harden, exhibit a yield stress peak due to the low mobility of superlattice dislocations coupling $\langle 100 \rangle$ faults.

Minor additions of certain elements have been shown to improve properties of iron aluminides. Of the elements listed in Table 2, chromium is most effective in increasing room-temperature ductility, niobium is most beneficial in improving the strength at elevated temperatures, and molybdenum appears to be best in improving creep resistance. The addition of TiB₂ to binary alloys produced a decrease in grain size of two to three times. However, preliminary studies indicate that these precipitates are deleterious to weldability. All the binary alloys and several of the ternary alloys experienced cracking in EB or GTA welds or both when TiB₂ was present. Many of these alloys prepared without TiB₂ did not have cracks. All alloys containing TiB₂ also had a mixed intergranular/transgranular cleavage fracture mode, but only transgranular cleavage when TiB₂ was not added. Because of these findings and the finding that grain refinement could be produced by minor additions of other elements (such as zirconium and niobium) that produce precipitates, the addition of TiB₂ as a grain-refinement technique has been halted.

Of the elements used for alloying studies, chromium appears to be the only one that can effectively improve the room-temperature ductility. Additions of 2-6% chromium produced ductilities of 7-10%, compared with 4% for the binary alloy. This improvement is decreased slightly, however, by further alloying with other elements. Further improvement in room-temperature ductility may result from controlling the microstructure through the rolling procedure and heat treatment.

Our work and that of other researchers indicate that there is good potential for both precipitation strengthening and solid-solution strengthening in iron aluminides.^{35,41} The addition of elements such as zirconium and niobium, which produces a precipitation-strengthening or dispersion-strengthening effect, was shown in our study to produce strengthening at temperatures near 600°C. Other studies have shown that elements such as molybdenum and titanium provide significant solid-solution strengthening up to 700°C by stabilizing the DO₃ structure with respect to the B2 structure.^{35,42}

In terms of creep resistance, molybdenum appears to be the best addition. The base binary alloy Fe-28% Al had a rupture life of less than 2 h at 207 MPa and 593°C in air, while additions of molybdenum produced improvements, with alloy FA-91 exhibiting the longest life (204 h).

Alloys based on Fe₃Al have excellent oxidation properties. The testing of alloys containing niobium and chromium at temperatures to 1000°C reveals no serious problems due to the addition of these elements. Also, static aqueous corrosion tests of annealed samples of chromium-containing alloys indicate that these alloys are highly resistant to corrosion in atmospheres with high moisture content.

The most promising alloys for future study appear to be those containing chromium, niobium, molybdenum, and boron. Our plans for this program involve selecting two multicomponent alloys for further composition refinement and properties studies. These alloys will be based on Fe-27±1% Al and will involve small additions of chromium, niobium, molybdenum, boron, and zirconium. The proper rolling and heat-treating schedule for optimizing the room-temperature ductility must be determined, and several heats will be prepared of each selected alloy to determine any heat-to-heat property variations.

7. REFERENCES

1. C. G. McKamey and C. T. Liu, "Development of Iron Aluminides for Gasification Systems," pp. 207-17 in *Proceedings of the Instrumentation, Components, and Materials Contractors Meeting*, DOE/METC-86/6069, U.S. Department of Energy, September 1986.
2. C. G. McKamey, C. T. Liu, S. A. David, and J. V. Cathcart, "Development of Iron Aluminides," pp. 45-52 in *Surface Gasification Materials Program Semiannual Progress Report for the Period Ending September 30, 1986*, ORNL/SGMP-86/2, January 1987.
3. C. G. McKamey, C. T. Liu, J. V. Cathcart, S. A. David, and E. H. Lee, *Evaluation of Mechanical and Metallurgical Properties of Fe₃Al-Based Aluminides*, ORNL/TM-10125, September 1986.
4. K. Oki, M. Hasaka, and T. Eguchi, *Jpn. J. Appl. Phys.* **12**(10), 1522 (1973).
5. P. W. Swann, W. R. Duff, and R. M. Fisher, *Trans. Am. Inst. Min. Metall. Pet. Eng.* **245**, 851 (1964).
6. H. Okamoto and P. A. Beck, *Metall. Trans.* **2**, 569 (1971).
7. S. A. Allen and J. W. Cahn, *Acta Metall.* **23**, 1017 (1975).
8. S. A. Allen and J. W. Cahn, *Acta Metall.* **24**, 425 (1976).
9. M. J. Marcinkowski and N. Brown, *Acta Metall.* **9**, 764 (1961).
10. N. S. Stoloff and R. G. Davies, *Acta Metall.* **12**, 473 (1964).
11. T. Saburi, I. Yamauchi, and S. Nenno, *J. Phys. Soc. Jpn.* **32**(3), 694 (1972).
12. S. K. Ehlers and M. G. Mendiratta, *Tensile Behavior of Fe-31 at. % Al Alloy*, AFWAL-TR-82-4089, Wright-Patterson Air Force Base, Ohio, 1982.
13. P. Morgand, P. Mouturat, and G. Sainfort, *Acta Metall.* **16**, 867 (1968).
14. C. T. Liu and J. O. Stiegler, *Science* **226**, 636 (1984).
15. Y. Umakoshi, M. Yamaguchi, Y. Namba, and K. Murakami, *Acta Metall.* **24**, 89 (1976).
16. M. J. Marcinkowski and D. S. Miller, *Philos. Mag.* **6**, 871 (1961).
17. B. H. Kear and H. G. Wilsdorf, *Trans. Am. Inst. Min. Metall. Pet. Eng.* **224**, 382 (1962).

18. S. Takeuchi and E. Kuramoto, *Acta Metall.* **21**, 415 (1973).
19. N. S. Stoloff and R. G. Davies, *Prog. Mater. Sci.* **13**, 1 (1966).
20. M. G. Mendiratta, S. K. Ehlers, and D. K. Chatterjee, "Tensile Behavior of RSR Iron-Aluminides," pp. 240-45 in *Proceedings of National Bureau of Standards Symposium on Rapid Solidification Processing, Principles and Technologies IV*, Dec. 6-8, 1982, Gaithersburg, Maryland.
21. H. J. Leamy and F. X. Kayser, *Phys. Status Solidi* **34**, 765 (1969).
22. R. C. Crawford and I.L.F. Ray, *Philos. Mag.* **35**(3), 549 (1977).
23. D. Hardwick and G. Wallwork, *Rev. High-Temp. Mater.* **4**, 47 (1978).
24. F. X. Kayser, *Iron-Aluminum Alloy Systems, Part 1, Fundamental Studies and Alloy Development*, WADC Technical Report 52-298, Wright Air Development Center, Wright-Patterson AFB, Ohio, May 1957.
25. W. Justusson, V. F. Zackay, and E. R. Morgan, *Trans. Am. Soc. Met.* **49**, 905 (1957).
26. G. Athanassiadis, G. Le Caer, J. Foct, and L. Rimlinger, *Phys. Status Solidi A* **40**, 425 (1977).
27. M. G. Mendiratta and H. A. Lipsitt, "DO₃-Domain Structures in Fe₃Al-X Alloys," pp. 155-62 in *Materials Research Society Symposia Proceedings, Vol. 39, High-Temperature Ordered Intermetallic Alloys*, ed. C. C. Koch, C. T. Liu, and N. S. Stoloff, Materials Research Society, Pittsburgh, 1985.
28. J. A. Horton, C. T. Liu, and C. C. Koch, "Alloying Effects and Microstructure of Iron-Aluminides," pp. 309-21 in *High-Temperature Alloys: Theory and Design*, ed. J. O. Stiegler, The Metallurgical Society of the American Institute of Mining, Metallurgical, and Petroleum Engineers, Warrendale, Pennsylvania, 1984.
29. J. F. Nachman and W. J. Buehler, *Thermenol, A Non-Strategic Aluminum-Iron Base Alloy for High Temperature Service*, NAVORD Report 3700, Naval Ordnance Laboratory, June 1954.
30. J. F. Nachman and W. J. Buehler, *Application, Properties, and Fabrication of Thermenol Type of Alloys*, NAVORD Report 4237, Naval Ordnance Laboratory, May 1956.
31. W. J. Lepkowski and J. W. Holladay, *The Present State of Development of Iron-Aluminum-Base Alloys*, Memorandum, Titanium Metallurgical Laboratory, Battelle Memorial Institute, Nov. 18, 1957.

32. J. W. Holladay, *Review of Development in Iron-Aluminum-Base Alloys*, DMIC Memo 82, Defense Metals Information Center, Battelle Memorial Institute, Columbus, Ohio, Jan. 30, 1961.
33. R. G. Bordeau, *Development of Iron Aluminides*, AFWAL-TR-87-4009, Air Force Wright Aeronautical Laboratories, Wright-Patterson Air Force Base, Ohio, May 1987.
34. G. Culbertson and C. S. Kortovich, *Development of Iron Aluminides*, AFWAL-TR-85-4155, Air Force Wright Aeronautical Laboratories, Wright-Patterson Air Force Base, Ohio, March 1986.
35. R. S. Diehm and D. E. Mikkola, "Effects of Mo and Ti Additions on the High Temperature Compressive Properties of Iron Aluminides near Fe_3Al ," pp. 329-34 in *Materials Research Society Symposia Proceedings, Vol. 81, High-Temperature Ordered Intermetallic Alloys, II*, ed. C. C. Koch, C. T. Liu, N. S. Stoloff, and O. Izumi, Materials Research Society, Pittsburgh, Pennsylvania, 1987.
36. H. Inouye, "Effects of DO_3 Transitions on the Yield Behavior of Fe-Al Alloys," pp. 255-61 in *Materials Research Society Symposia Proceedings, Vol. 39, High-Temperature Ordered Intermetallic Alloys*, ed. C. C. Koch, C. T. Liu, and N. S. Stoloff, Materials Research Society, Pittsburgh, Pennsylvania, 1985.
37. M. G. Mendiratta, H.-M. Kim, and H. A. Lipsitt, *Metall. Trans. A15*, 395 (1984).
38. C. G. McKamey, J. A. Horton, and C. T. Liu, "Effect of Aluminum Addition on Ductility and Yield Strength of Fe_3Al Alloys with 0.5 wt % TiB_2 ," pp. 321-27 in *Materials Research Society Symposia Proceedings, Vol. 81, High-Temperature Ordered Intermetallic Alloys, II*, ed. C. C. Koch, C. T. Liu, N. S. Stoloff, and O. Izumi, Materials Research Society, Pittsburgh, Pennsylvania, 1987.
39. M. J. Marcinkowski and N. Brown, *J. Appl. Phys.* **33**(2), 537 (1962).
40. C. G. McKamey and J. A. Horton, "The Effect of Molybdenum Addition on Properties of Iron Aluminides," to be published in *Met. Trans.*

41. M. G. Mendiratta, S. K. Ehlers, D. M. Dimiduk, W. R. Kerr, S. Mazdidasni, and H. A. Lipsitt, "A Review of Recent Developments in Iron Aluminides," pp. 393-404 in *Materials Research Society Symposia Proceedings, Vol. 81, High-Temperature Ordered Intermetallic Alloys, II*, ed. C. C. Koch, C. T. Liu, N. S. Stoloff, and O. Izumi, Materials Research Society, Pittsburgh, Pennsylvania, 1987.

42. R. T. Fortnum and D. E. Mikkola, *Mater. Sci. Eng.* **91**, 223 (1987).

INTERNAL DISTRIBUTION

- | | | | |
|--------|-------------------------------|--------|-----------------------------|
| 1-2. | Central Research Library | 44-48. | C. G. McKamey |
| 3. | Document Reference Section | 49. | T. A. Nolan |
| 4-5. | Laboratory Records Department | 50. | W. C. Oliver |
| 6. | Laboratory Records, ORNL RC | 51. | D. F. Pedraza |
| 7. | ORNL Patent Section | 52-56. | D. H. Pierce |
| 8. | R. L. Beatty | 57. | W. D. Porter |
| 9. | P. J. Blau | 58. | P. L. Rittenhouse |
| 10. | R. A. Bradley | 59. | A. C. Schaffhauser |
| 11-15. | J. J. Campbell | 60. | V. K. Sikka |
| 16. | P. T. Carlson | 61. | G. M. Slaughter |
| 17. | G. L. Copeland | 62. | J. O. Stiegler |
| 18. | D. F. Craig | 63. | R. W. Swindeman |
| 19-23. | S. A. David | 64-68. | P. T. Thornton |
| 24. | J. H. DeVan | 69. | P. F. Tortorelli |
| 25. | C. K. DuBose | 70. | J. R. Weir |
| 26. | J. I. Federer | 71. | F. W. Wiffen |
| 27. | E. P. George | 72. | D. F. Wilson |
| 28. | G. M. Goodwin | 73. | A. Zucker |
| 29-33. | J. A. Horton | 74. | H. D. Brody (Consultant) |
| 34. | G. C. Hsueh | 75. | G. Y. Chin (Consultant) |
| 35. | R. R. Judkins | 76. | F. F. Lange (Consultant) |
| 36. | J. R. Keiser | 77. | W. D. Nix (Consultant) |
| 37. | H. E. Kim | 78. | D. P. Pope (Consultant) |
| 38. | O. F. Kimball | 79. | E. R. Thompson (Consultant) |
| 39-43. | C. T. Liu | | |

EXTERNAL DISTRIBUTION

- 80-81. AIR FORCE WRIGHT AERONAUTICAL LABORATORIES, Metals and Ceramics
Division, Wright-Patterson Air Force Base, OH 45433
D. M. Dimiduk
W. R. Kerr
82. AMAX R&D CENTER, 5950 McIntyre St., Golden, CO 80403
T. B. Cox
83. AMERICAN WELDING SOCIETY, 550 LeJeune Road, Miami, FL 33126
H. G. Ziegenfuss
84. ARGONNE NATIONAL LABORATORY, Materials Science and Technology
Division, 9700 S. Cass Ave., Argonne, IL 60439
K. Natesan

85. BABCOCK & WILCOX COMPANY, 20 S. Van Buren Ave., Barberton,
OH 44203
Michael Gold
86. CABOT CORP., Technology Dept., 1020 W. Park Avenue, Kokomo, IN
46901
A. Asphahani
87. CASE WESTERN RESERVE UNIVERSITY, Dept. of Metallurgical &
Materials Science, 10900 Euclid Avenue, Cleveland, OH 44106
K. Vedula
88. COMBUSTION ENGINEERING, INC., 911 W. Main Street, Chattanooga,
TN 37401
D. A. Canonico
89. CORNELL UNIVERSITY, Ithaca, NY 14850
Che-Yu Li
- 90-91. ELECTRIC POWER RESEARCH INSTITUTE, P.O. Box 10412, Palo Alto,
CA 94303
W. T. Bakker
J. T. Stringer
92. EXXON RESEARCH AND ENGINEERING COMPANY, Clinton Township, Route 2
East, Annadale, NJ 08801
M. L. Gorbaty
93. FOSTER WHEELER DEVELOPMENT CORPORATION, 12 Peach Tree Hill
Road, Livingston, NJ 07939
J. L. Blough
- 94-95. GARRETT TURBINE ENGINE COMPANY, Advanced Materials, Materials
Engineering, 111 South 34 Street, P.O. Box 5217, Phoenix, AZ
85010
G. S. Hoppin
B. Keiser
96. GA TECHNOLOGIES, P.O. Box 81608, San Diego, CA 92138
D. I. Roberts
- 97-98. GENERAL ELECTRIC COMPANY, Bldg. 81, Rm. E102, Schenectady, NY
12345
S. C. Huang
A. I. Taub

99. GENERAL ELECTRIC COMPANY, Quartz and Chemicals Dept.,
24400 Highland Road, Richmond Heights, OH 44413
G. W. Weber
100. GENERAL MOTORS RESEARCH, Metallurgical Department, Warren, MI
48090-9055
Susan Schron
101. GEORGIA INSTITUTE OF TECHNOLOGY, School of Materials Engineering,
Bunger-Henry Bldg., Atlanta, GA 30332
S. Antolovich
102. INSTITUTE OF DEFENSE ANALYSES, 1801 Beauregard Street,
Alexandria, VA 22311
T. F. Kearns
103. LEHIGH UNIVERSITY, Materials Research Center, Bethlehem, PA 18015
Y. T. Chou
- 104-105. LOCKHEED CORPORATION, Palo Alto Laboratories, 3251 Hanover St.,
Palo Alto, CA 94304
E. C. Burke
R. A. Perkins
106. THE MATERIALS PROPERTIES COUNCIL, INC., 345 E. Forty-Seventh
Street, New York, NY 10017
M. Prager
107. MONSANTO COMPANY, P.O. Box 1311, Texas City, TX 77590
P. S. Gupton
108. NAVAL SURFACE WEAPONS CENTER, Code R32, White Oak, Silver Spring,
MD 20910
H. M. DeJarnette
109. NAVAL SURFACE WEAPONS CENTER, Surface Weapons Materials
Technology Program, Dahlgren, VA 22448
W. T. Messick
110. NORTH CAROLINA STATE UNIVERSITY, Materials Engineering Dept.,
Raleigh, NC 27650
C. C. Koch
111. OAK RIDGE ASSOCIATED UNIVERSITIES LIBRARY, Oak Ridge, TN 37831
MERT Division

112. RENSSELAER POLYMER INSTITUTE, Materials Engineering Dept.,
Troy, NY 12181
N. S. Stoloff
113. R. L. Smith, P.O. Box 98, Chassel, MI 49916
114. G. Sorell, 123 Smull Ave., West Caldwell, NY 07006
115. UNIVERSAL CYCLOPS SPECIALTY STEEL DIVISION, 650 Washington Road,
Pittsburgh, PA 15228
H. L. Black
116. UNIVERSAL ENERGY SYSTEMS, INC., 4401 Dayton-Xenia Road,
Dayton, OH 45432
M. G. Mendiratta
117. UNIVERSITY OF MASSACHUSETTS, Department of Polymer Science,
Room 701, GRC, Amherst, MA 01003
R. S. Porter
118. UNIVERSITY OF TENNESSEE, Materials Science and Engineering
Department, Knoxville, TN 37916
C. R. Brooks
119. VANDERBILT UNIVERSITY, Station B, P.O. Box 1621,
Nashville, TN 37235
J. J. Wert
120. VIRGINIA POLYTECHNIC INSTITUTE AND STATE UNIVERSITY,
Blacksburg, VA 24061
D. A. Farkas
- 121-122. DOE, ENERGY SYSTEMS RESEARCH AND DEVELOPMENT, Office of
Conservation and Renewable Energy, Forrestal Building
Independence Avenue, Washington, DC 20585
J. J. Brogan
J. J. Eberhardt
- 123-124. DOE, OFFICE OF FOSSIL ENERGY, Washington, DC 20545
J. P. Carr, FE-14, Room E322, GTN
M. I. Singer, FE-14, MS B115, GTN
R. T. King, MS B115, GTN

125. DOE, OAK RIDGE OPERATIONS OFFICE, P.O. Box E, Oak Ridge, TN 37831
Office of Assistant Manager for Energy Research and
Development
- 126-127. DOE, MORGANTOWN ENERGY TECHNOLOGY CENTER, P.O. Box 880,
Morgantown, WV 26505
D. Dubis
J. Byam
- 128-137. DOE, OFFICE OF SCIENTIFIC AND TECHNICAL INFORMATION,
P.O. Box 62, Oak Ridge, TN 37831
For distribution by microfiche as shown in DOE/TIC-4500,
Distribution Categories UC-103 (Fluidized Bed Combustion,
UC-109 [Coal Gasification (Surface and Underground)],
and UC-114 (Coal-Based Materials and Components)

✓

1

0

1

✓

✓